REPORT DOCUMENTATION PAGE

Form Approved
OMB NO. 0704-0188

1. AGENCY USE ONLY (Leave Blank)	2. REPORT DATE	3. REPORT TYPE AND DATES COVERED
	27 November 2000	Final Progress: 1 September 1996 - 30 June 2000

4. TITLE AND SUBTITLE
Systems Design of Hierarchically Structured Materials

5. FUNDING NUMBERS
DAAH04-96-1-0266

6. AUTHOR(S)
G. B. Olson

7. PERFORMING ORGANIZATION NAME(S) AND ADDRESS(ES)
Northwestern University
633 Clark Street
Evanston, IL 60208-1110

8. PERFORMING ORGANIZATION REPORT NUMBER

9. SPONSORING / MONITORING AGENCY NAME(S) AND ADDRESS(ES)
U. S. Army Research Office
P.O. Box 12211
Research Triangle Park, NC 27709-2211

10. SPONSORING / MONITORING AGENCY REPORT NUMBER
ARO 35743.4 -MS

11. SUPPLEMENTARY NOTES
The views, opinions and/or findings contained in this report are those of the author(s) and should not be construed as an official Department of the Army position, policy or decision, unless so designated by other documentation.

12 a. DISTRIBUTION / AVAILABILITY STATEMENT
Approved for public release; distribution unlimited.

12 b. DISTRIBUTION CODE

13. ABSTRACT (Maximum 200 words)

Research extended the SRG systems design approach to more complex materials by establishing methodology and fundamental principles for rational design of higher levels of structural hierarchy, while incorporating increased dynamic character in the form of adaptive system concepts via synergistic integration of materials science and applied mechanics. Research addressed both the methodology of rational design at new levels of materials complexity, and the fundamental principles of specific materials behaviors necessary to support quantitative design. This included principles of microstructural evolution during coherent carbide precipitation for efficient strengthening without embrittlement, control of metastable austenite precipitation for optimal-stability transformation toughening, behavior of pseudoelastic crack-bridge toughening, and shape-memory-based healing of internal composite damage. Exploratory research also addressed conceptual design of multifunctional metal/ceramic hybrid armor systems, and transformation-plasticity based matrix alloys for shearable tungsten heavy alloy composites.

14. SUBJECT TERMS
materials design

15. NUMBER OF PAGES
25

16. PRICE CODE

17. SECURITY CLASSIFICATION OR REPORT	18. SECURITY CLASSIFICATION ON THIS PAGE	19. SECURITY CLASSIFICATION OF ABSTRACT	20. LIMITATION OF ABSTRACT
UNCLASSIFIED	UNCLASSIFIED	UNCLASSIFIED	UL

Participating Scientific Personnel

Prof. Gregory B. Olson, Principal Investigator
Prof. Brian Moran, Co-Investigator
Dr. Gautam Ghosh, Asst. Res. Professor
Yasunobu Nagataki, Visiting Scientist
Richard Kraemer, Technician
Christopher Kantner, Research Assistant
Bradley Files, Research Assistant (PhD December 1997)
John Wise, Research Assistant (PhD June 1998)
James Wright, Research Assistant
Deborah Burton, AASERT Fellow
Priscilla Bernikowicz, Undergraduate Researcher
Christopher Scharff, Undergraduate Researcher
Brian Tufts, Undergraduate Researcher
Scott Roth, Undergraduate Researcher

Report of Inventions

"Ultrahard Carburizing Secondary Hardening Steels," pending.

Participating Scientific Personnel

Prof. Gregory B. Olson, Principal Investigator
Prof. Brian Moran, Co-Investigator
Dr. Gautam Ghosh, Asst. Res. Professor
Yasunobu Nagataki, Visiting Scientist
Richard Kraemer, Technician
Christopher Kantner, Research Assistant
Bradley Files, Research Assistant (PhD December 1997)
John Wise, Research Assistant (PhD June 1998)
James Wright, Research Assistant
Deborah Burton, AASERT Fellow
Priscilla Bernikowicz, Undergraduate Researcher
Christopher Scharff, Undergraduate Researcher
Brian Tufts, Undergraduate Researcher
Scott Roth, Undergraduate Researcher

Report of Inventions

"Ultrahard Carburizing Secondary Hardening Steels," pending.

Final Report

System Design of Hierarchically Structured Materials

Submitted to Army Research Office

G. B. Olson
Northwestern University

Executive Summary of the Research

Research extended the SRG systems design approach to higher levels of structural hierarchy, while incorporating dynamic character in the form of adaptive system concepts via a synergistic integration of materials science and applied mechanics. The research addressed both the methodology of rational design at new levels of materials complexity, and the fundamental principles of specific materials behaviors necessary to support quantitative design. The research addressed adaptive multilevel microstructures in two broad areas for applications of advanced alloys:

(a) Gradient and Layered Systems with application in high performance gear technology and advanced dual-hardness armor, achieving novel strength/toughness combinations through control of coherent carbide precipitation in processing and tuned-stability crack tip transformation plasticity in service.
(b) Biomimetic Laminate Systems combining an oxidation resistant and high-temperature creep resistant matrix alloy with a thermodynamically compatible ductile reinforcement consisting of a shape memory alloy imparting biologically-inspired ductile-crack-bridge toughening via thermoelastic martensite pseudoelasticity at low temperatures, and shape-memory-induced crack clamping for diffusional damage healing at high temperatures.

The primary objectives of the research effort were the methodology and fundamental principles for rational design of complex materials. This included the principles of microstructural evolution during coherent carbide precipitation for efficient strengthening without embrittlement, the control of metastable austenite precipitation for optimal-stability transformation toughening, the behavior of pseudoelastic crack-bridge toughening, and the shape-memory-based healing of internal composite damage. Research emphasized the dynamics of microstructural evolution during processing and in service, and the design methodology for control of multilevel dynamic hierarchical microstructures as programmed adaptive systems.

Specific property targets that guided the conceptual design of prototype materials for evaluation were: 1) A secondary hardening gear steel with a case hardness of R_C70 while maintaining the core of $K_{IC} > 60$ MPa $m^{1/2}$ at R_C 50 hardness up to 400 °C. 2) A dual hardness armor system with a front face hardness of R_C 65-70, and a transformation toughened back plate of R_C 55-57 and $K_{IC} > 80$ MPa $m^{1/2}$. 3) A shape-memory reinforced superalloy laminate system with a 10^5 hr creep strength of 100 MPa at an operating temperature 600-700 °C.

Exploratory research also addressed the conceptual design of multifunctional metal/ceramic hybrid armor systems, and transformation-plasticity based matrix alloys for shearable tungsten heavy alloy composites.

Background

Materials as Hierarchical Systems

The late C. S. Smith [1] expounded a "systems" view of materials as hierarchical structures with properties governed by dynamic evolution in processing and in service. The Smith philosophy has been developed into a methodology for rational design of complex materials, pioneered by the multi-institutional Steel Research Group (SRG) program centered at Northwestern University [2-4], demonstrating successful application in high toughness ultrahigh-strength alloy steels [4,5]. This view of a secondary-hardening martensitic alloy steel as a system is summarized in Figure 1 and 2 [2], depicting the hierarchy of microstructural subsystems controlling the required set of properties for desired performance, and the sequential processing subsystems which in turn control structure. The system chart for high power density gear systems, Figure 2, considers not only the case/core gradient system of the gear steel itself, but the integrated design of compatible superhard ceramic coatings and their interfaces, ultimately incorporating redesign of gear shape to optimally exploit new material properties. Also represented are alternative processing routes to provide affordable manufacturing strategies for specific applications. Organized within this framework, basic research integrating materials science, applied mechanics and quantum physics has focused on key process/structure and structure/property relations, defining quantitative microstructural objectives expressible in thermodynamic terms (including scaling factors governing dynamic evolution), and the THERMOCALC thermochemical database and software system [6] has been applied as an integrative design tool predicting multi-component alloy composition capable of achieving desired multiphase microstructures under prescribed processing conditions. The successful application of this approach in ultrahigh strength steels has made possible an undergraduate course in Materials Design [3], and the extension of thermodynamics-based systems design to ceramics and polymers is now being undertaken within the Department of Materials Science and Engineering at Northwestern [7].

C. S. Smith also emphasized the strong parallels between engineering materials and the hierarchical structures of the biological world [1,8]. The discovery that relatively primitive biological systems such as viruses and bacteria exploit such sophisticated materials technology as martensitic transformation plasticity and the shape memory effect [9] reinforces this parallelism. In response, an active area of current investigation is the field of biomimetics [10,11] in which complex biological systems are investigated to incorporate biological principles in the rational design of more sophisticated engineering materials. This has inspired the notion of extending materials structure to both higher levels of hierarchy and more dynamic character to achieve "adaptive" or "smart" microstructures programmed to evolve along predetermined pathways in response to a given stimulus to achieve novel properties. Such programming "brings to life" Smith's seminal vision of dynamic hierarchical materials.

The Steel Research Group

The science-based approach to the computational systems design of materials is based on the pioneering work of the multi-institutional interdisciplinary Steel Research Group (SRG) program directed by G. B. Olson. Initiated in 1985 under NSF support as a collaboration of MIT, Harvard, and Brown with government laboratories and industry, the SRG reorganized in 1988 with Northwestern as lead institution, funded by mission-oriented agencies including ARO, ONR, AFOSR, NASA and DOE with approximately 20% industry support, and continuing NSF supercomputing support. Progress in the first 5 years is summarized in the Proceedings of the 34th Sagamore Army Materials Research Conference [12], organized around the SRG effort. The SRG design approach integrating processing/ structure/property/performance relations within a multilevel hierarchical system structure, and the computational design tools stemming from the research integrating quantum physics, applied mechanics and materials science are described in a recent invited overview [13] and millennial essay [13a] for *Science* magazine, attached as Appendix A. Broadening the approach to design of all

materials was the subject of a recent Gordon Research Conference [14] and a recent international symposium on materials design [14a].

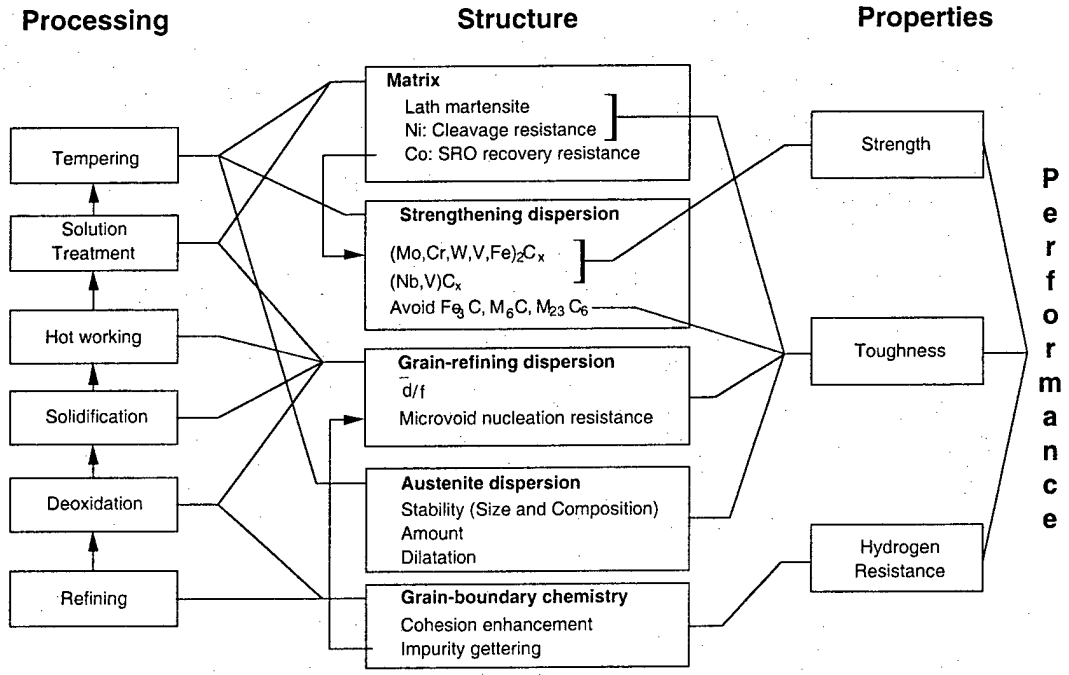

Figure 1. System structure of secondary hardening martensitic alloy steel.

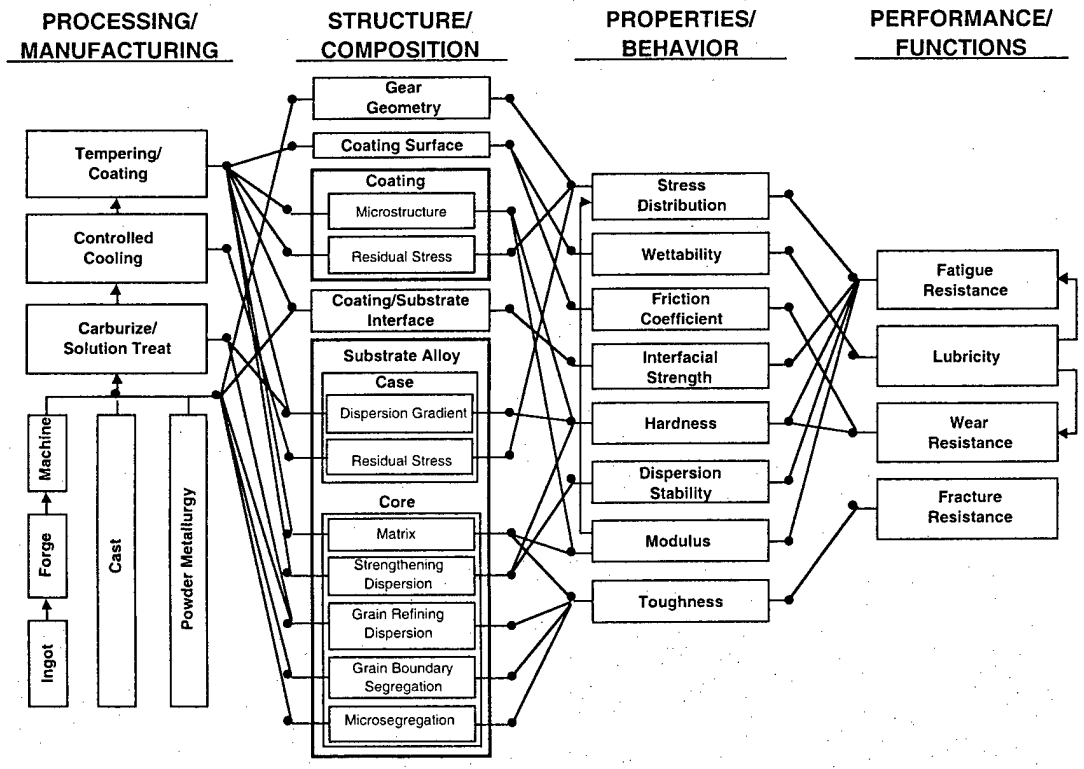

Figure 2. **System structure of high power-density gears.**

The design methodology

As discussed further in Appendix A, Figures 1 and 2 concisely summarize the systems approach unifying our design methodology. The chart denotes the hierarchy of microstructural subsystems underlying the set of material properties necessary for desired performance, and the sequential stages of processing which govern their dynamic evolution. This systems view identifies and prioritizes the key structure/property and process/structure relations for which computational models are needed to support predictive design. The resulting hierarchy of computational tools is summarized in Appendix A (insert, p. 997). Dynamic models predict evolution of microstructure in both processing and service. Working down from the highest structural level, models support (a) *transformation design* controlling the evolution of martensitic microstructures and their dynamic competition with alternative diffusional transformations, (b) *micromechanics design* via simulation of unit fracture processes in service employing kinetics-based constitutive laws (c) *nanodesign* integrating continuum mechanics of interfacial coherency and capillarity with multicomponent diffusional precipitation kinetics for efficient strength control, and (d) *quantum design* integrating frontier computational quantum mechanics in control of interfacial adhesion phenomena underlying higher level behaviors. Output of these tools defines thermodynamic design parameters governing critical time and length scales, allowing use of the THERMOCALC thermochemical software and database system as the principal design integration tool to satisfy multiscale design requirements. The efficacy of the approach has now been demonstrated in numerous SRG designs described in Appendix A and several review articles [15-18]. The Materials-by-Design doctrine has gained international recognition [19].

Achievements

Education Initiatives

As MSE Associate Chairman, Prof. Olson led a committee which restructured the department curriculum, preparing students to take Materials Design in the Junior year. A Senior level Process Design course developed by D. L. Johnson featuring process optimization via statistical design of experiments, is followed by a 2-quarter experimental Senior Project. This structure allows students to perform theory-based conceptual designs in the Junior year and evaluate their prototype material as a Senior Project using experimental methods of the Process Design course. The new design-oriented curriculum has been credited for Northwestern's program tying MIT in the most recent US News and World Report rankings. As a member of the Engineering First Committee restructuring the early undergraduate engineering curriculum, Olson brought computational materials design projects to a new Freshman-level 2 quarter Engineering Design and Communications course, building on experience with high school student summer projects. A freshman team successfully designed and implemented a Sn-based shape-memory-reinforced self healing biomimetic alloy composite. The growing design culture has brought student entrepreneurship to the undergraduate level. A team of freshman design students who performed a software project started a website design company during their freshman year, and the organizational meeting of an Enterprise Club drew over 100 interested engineering students. In the past year, the club organized an Enterprise course that drew 90 students, culminating in presentation of their business plans to investors.

The SRG brought a close synergy of research and teaching with the development of Olson's MSc C90 Materials Design course at Northwestern [3]. Student team projects in which undergraduates employ THERMOCALC computational thermodynamics to integrate results of SRG graduate research have won national student materials design competitions [20-23] and have been featured on PBS-TV [24], several magazine articles [25-27], and a recent popular book on materials [28]. Projects have involved collaboration with design classes in other departments in the schools of engineering and management, and establishment of a similar materials design course in Sweden fostered through doctoral student exchange has allowed international undergraduate

collaboration via internet [29]. Management school collaboration has facilitated student entrepreneurship through market analysis and business plans. After graduation, Dr. Charles Kuehmann founded QuesTek Innovations LLC offering computational alloy design services based on SRG technology, and new commercial alloys are undergoing field tests. In December 1999, QuesTek received the Technology of the Year Award from Industry Week magazine, in recognition of the new "materials by design" technology.

Fundamental principles for design of complex materials

1. Strengthening

The first dynamic problem of interest in the systems of Figures 1 and 2 is the evolution of coherent carbide precipitation controlling strength. The pioneering work of Speich [30] established that good toughness in secondary hardening alloy steels demands near-completion of M_2C alloy carbide precipitation in order to dissolve transient cementite (Fe_3C) particles that otherwise contribute to microvoid nucleation during ductile fracture. The challenge to maintaining strength in such an overaged condition is to maintain a fine carbide particle size. A thorough electron microscopy study of M_2C precipitation in the commercial AF1410 steel [31] was performed in the doctoral research of J. S. Montgomery (now at ARL/WMD) in conjunction with Small Angle Neutron Scattering (SANS) studies by Weertman and coworkers [32], demonstrating coherent precipitation behavior consistent with recent theory of precipitation at high supersaturations [33,34]. In this regime the fundamental scaling factor governing particle size (and thus alloy strength) is the initial critical nucleus size which scales inversely with the thermodynamic driving force for precipitation; the time scale of precipitation is governed by a diffusion time defined by the coarsening rate constant. To compute the thermodynamic driving force for coherent M_2C precipitation, the doctoral research of K. C. King with Professors T. Mura and P. Voorhees addressed the elastic self energy of the coherent carbides [35], and also explored the elastic interactions with dislocations during heterogeneous nucleation [36]. Incorporating the composition dependence of the carbide lattice parameters, the THERMOCALC chemical thermodynamic database [22] was then modified to incorporate the additional elastic self energy contribution to the thermodynamics of coherent precipitation. To control the time scale of precipitation, theories of coarsening kinetics in multicomponent systems were developed by Kuehmann & Voorhees [37] and Umantsev [38] to define a multicomponent diffusional rate constant.

Our recent work has tested model predictions in a series of 16Co-5Ni-0.24C steels with the Cr and Mo contents represented in Figure 3 displaying a contour plot of predicted coherent precipitation driving force. An X-ray diffraction study of the precipitation hardening behavior of these alloys was initiated by Visiting Scientist S. Endo of NKK Japan and correlated with model predictions by Research Scientist C. J. Kuehmann [4]. Measured peak hardness showed a strong correlation with the coherent precipitation driving force after taking into account the "paraequilibrium" condition of prior precipitation of cementite under carbon diffusion control.

Toward improved precision of the M_2C coherent thermodynamics, the doctoral research of C. Knepfler [39,40], with ceramist Prof. K. Faber, addressed the synthesis and characterization of $(Mo,Cr,V,Fe)_2C$ carbides in bulk form, measuring the composition dependence of lattice parameters, thermal expansion and isotropic elastic moduli as inputs into a more precise treatment of the composition and temperature dependence of the carbide elastic self energy. Measured elastic constants were also applied to an analysis of the critical particle size for the shear/bypass transition in precipitation strengthening of steels.

The doctoral research of R-H. Liarng [41] with Prof. Mura incorporated Knepfler's measurements in refined calculations of the carbide elastic self energy in an iron-based matrix, taking into account the differing elastic constants of matrix and particle, and the role of particle shape. Liarng also computed internal stresses on carbide shear systems relevant to coherency loss mechanisms, predicted solute distributions around coherent particles,

and considered interparticle elastic interactions promoting autocatalytic nucleation. As the transformation eigenstrains for a coherent M_2C carbide in an Fe matrix are quite high, these linear elastic calculations are regarded as upper bound estimates of self energies and local stresses. To rationalize observed coherent nucleation conditions and coherent particle compositions measured by atom-probe microanalysis, it has been necessary to apply a correction factor of about 1/3 to the computed self energies. Liarng performed lower bound self energy estimates by excluding the energy density contributions of highly strained regions likely to be strongly nonlinear, similar to the dislocation core cutoff approximation, supporting correction factors of this magnitude. More recently, preliminary nonlinear numerical calculations by Graduate Fellow L. Coates working with Prof. Brian Moran offered further support for the reduced elastic energy.

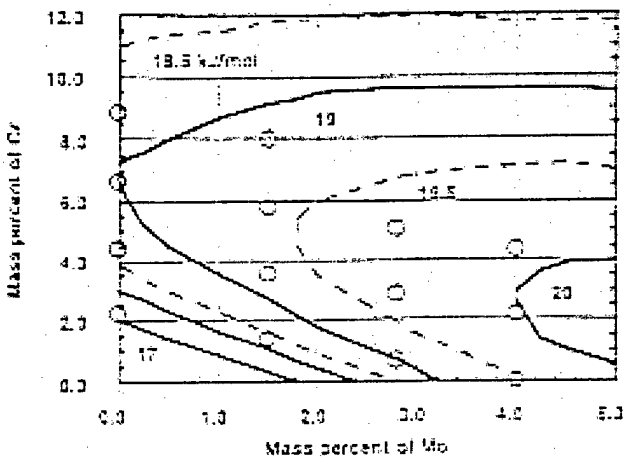

Figure 3. Contour plots of predicted coherent M_2C precipitation driving force for 16Co-5Ni-0.24C steels at 510 °C vs. Cr and Mo content. Open points denote compositions of experimental alloy series.

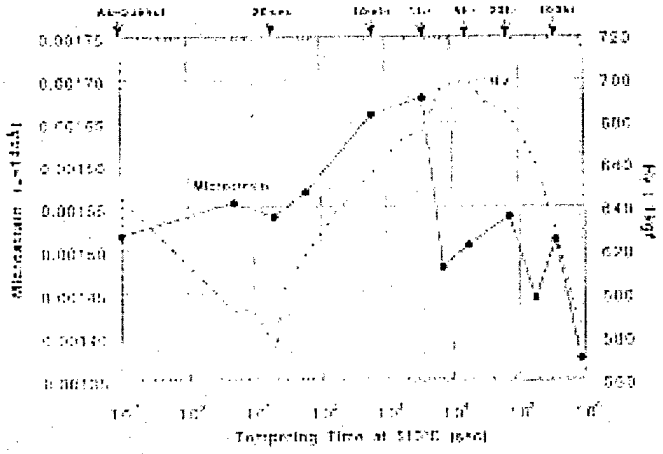

Figure 4. Evolution of microstrain distribution width (measured with Fourier column length of L=144Å) with 510°C tempering of 16Co5Ni4Cr4Mo0.24C steel. Dashed curve depicts Vickers hardness (right scale).

In our most recent work, Visiting Scientist Y. Nagataki of NKK Corporation collaborated with the late Prof. J. B. Cohen [42] to perform precision X-ray line broadening studies to quantify both dislocation recovery during tempering and the evolution of matrix micro-strain associated with carbide coherency. The latter is represented as a function of tempering time in Figure 4 for the case of the highest driving force composition (4Cr4Mo) of Figure 3. The dashed curve representing Vickers hardness (right scale) shows that maximum coherency micro-strain occurs just before peak hardness. From corresponding SANS measurements of particle size, this identifies a critical particle size for coherency loss of 3nm.

Treating the high-supersaturation precipitating system as an evolving unstable equilibrium, Research Fellow Carrie Campbell [43,44] integrated the diverse experimental data to correlate particle size (corrected for shape dependence of capillary energy) with thermodynamic driving force defined by measured phase fraction, as represented in Figure 5 for the example of the 4Mo alloy of the series of Figure 3. Slopes define interfacial energies for the coherent (below 3nm size) and incoherent states of the M_2C carbides, supporting an elastic energy correction factor of 0.4 (as described earlier) to give the linear behavior shown for the coherent state. With these parameters, the thermodynamic database can predict the full trajectory of particle size, phase fraction and phase composition during precipitation.

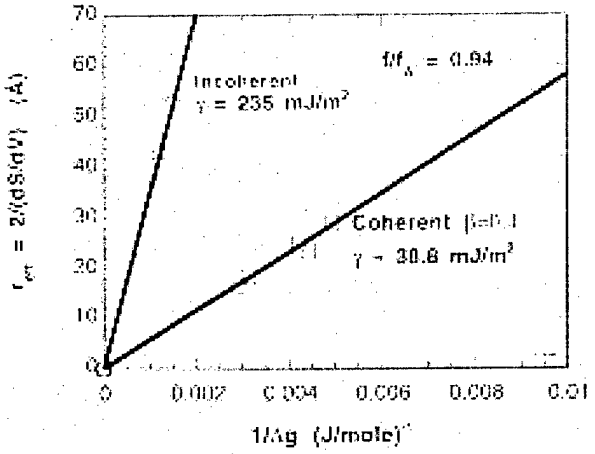

Figure 5. Correlation of measured effective particle size (corrected for shape dependence of capillarity) with reciprocal driving force, defining interfacial energy for coherent and incoherent M_2C carbides in 16Co5Ni4Mo0.24C steel.

Table 1: The strengthening mechanisms

Solid solution strengthening	$\sigma_{ss} = ZG(\lvert\dot{\varepsilon}_G\rvert + \alpha\lvert\dot{\varepsilon}_a\rvert)^{4/3}c^{2/3}$
Particle strengthening, shear cutting	$\sigma_{P,shear} = 0.56\frac{Gb}{L-2R}\left(\frac{G_pR}{2\pi Gb}\right)^{3/2}$
Particle strengthening, Orowan bypass	$\sigma_{P,Orowan} = 1.7\frac{Gb}{2\pi(1-\nu)^{1/2}(L-2R)}ln\left(\frac{2R}{r_0}\right)$
Martensitic interfacial strengthening	$\sigma_{\alpha'} = \sigma_{Fe} + \sum_i m_i\left(\bar{L}_i\right)^{-1/2}$
Dislocation substructure strengthening	$\sigma_D = k\mu b\rho_D^{1/2} = b - aln(t) \approx \sigma_D^0 - \Delta\sigma_D^R\left(\frac{V}{V_f}\right)$

Research Assistant John Wise [45,46] incorporated the precipitation trajectory model into a strengthening model by calibrating the contributions of solution strengthening (σ_{SS}), particle strengthening (σ_P), martensitic interfacial strengthening ($\sigma_{\alpha'}$), and dislocation substructure strengthening (σ_D) as represented by the equations listed in Table 1 and calibrated from Small Angle Neutron Scattering (SANS) data in Figure 6. The figure show the calibration of the strengthening contributions of shearable and nonshearable (Orowan) obstacles to the SANS measurements. Using the measured particle size distributions, the analysis gives a critical particle size for the shear to bypass transition of 3nm, equivalent to the critical size for coherency loss. Figure 7 summarizes the evolution of predicted hardness with relative phase fraction (normalized to the final equilibrium fraction) for four of the alloys of Figure 3. The predictions are in excellent agreement with experiment, and show that higher

driving force compositions achieve greater peak hardness by reaching the critical shear/bypass size at higher relative phase fractions.

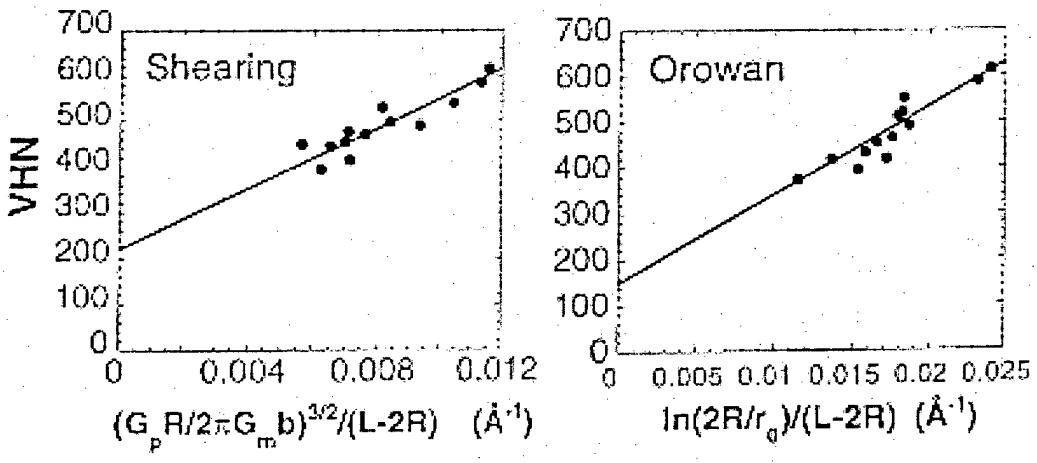

Figure 6. Strengthening model equations employed for secondary hardening martensitic steels. Lower figures show calibrations of particle strengthening contributions of shearable and unshearable (Orowan) obstacles from SANS data.

Research Associate Dr. Gautam Ghosh [47] has performed an analytical electron microscopy study demonstrating the paraequilibrium state of cementite (formed without substitutional diffusion) prior to M_2C precipitation, and has quantified the early stages of cementite composition change during M_2C precipitation. The evolution of cementite composition is important to evolution of the matrix carbon potential, which exerts a strong influence on the driving force controlling M_2C particle size. Toward tighter control of precipitation strengthening, a quantitative modeling of cementite/matrix substitutional solute partitioning using the DICTRA multicomponent diffusion code is needed.

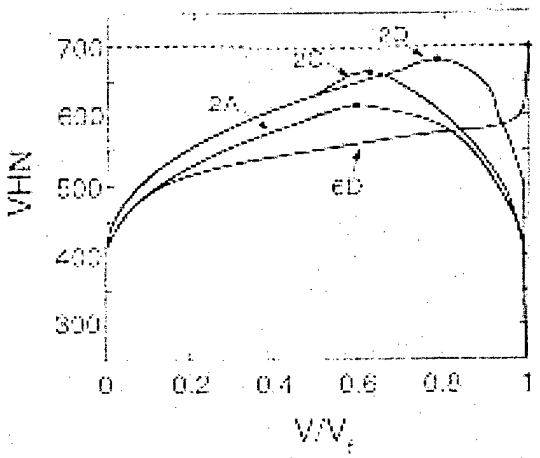

Figure 7. Predicted evolution of hardness with relative carbide phase fraction in secondary hardening 16Co5Ni0.24C steels of varying Cr and Mo content.

The evolution of M_2C particle composition during coherent precipitation is very important to the calibration of elastic self energy models. A new opportunity for more rapid measurement of particle composition at the important 1-3 nm size scale is the establishment of a high mass resolution 3D atom probe at Northwestern based on a new design from Oxford University commercialized by Kindbrisk, Ltd. Testing of the new instrument at Oxford produced the reconstructed 3D images in Figure 8 for the 0.24C-16Co-5Ni-4Cr-4Mo steel in the peak hardness condition. The image highlights matrix Fe, Co and Ni and the carbide Cr, Mo and C. With discrete

crystal planes clearly evident, the 3 nm carbide corresponds to the critical size for coherency loss and shear/bypass transition.

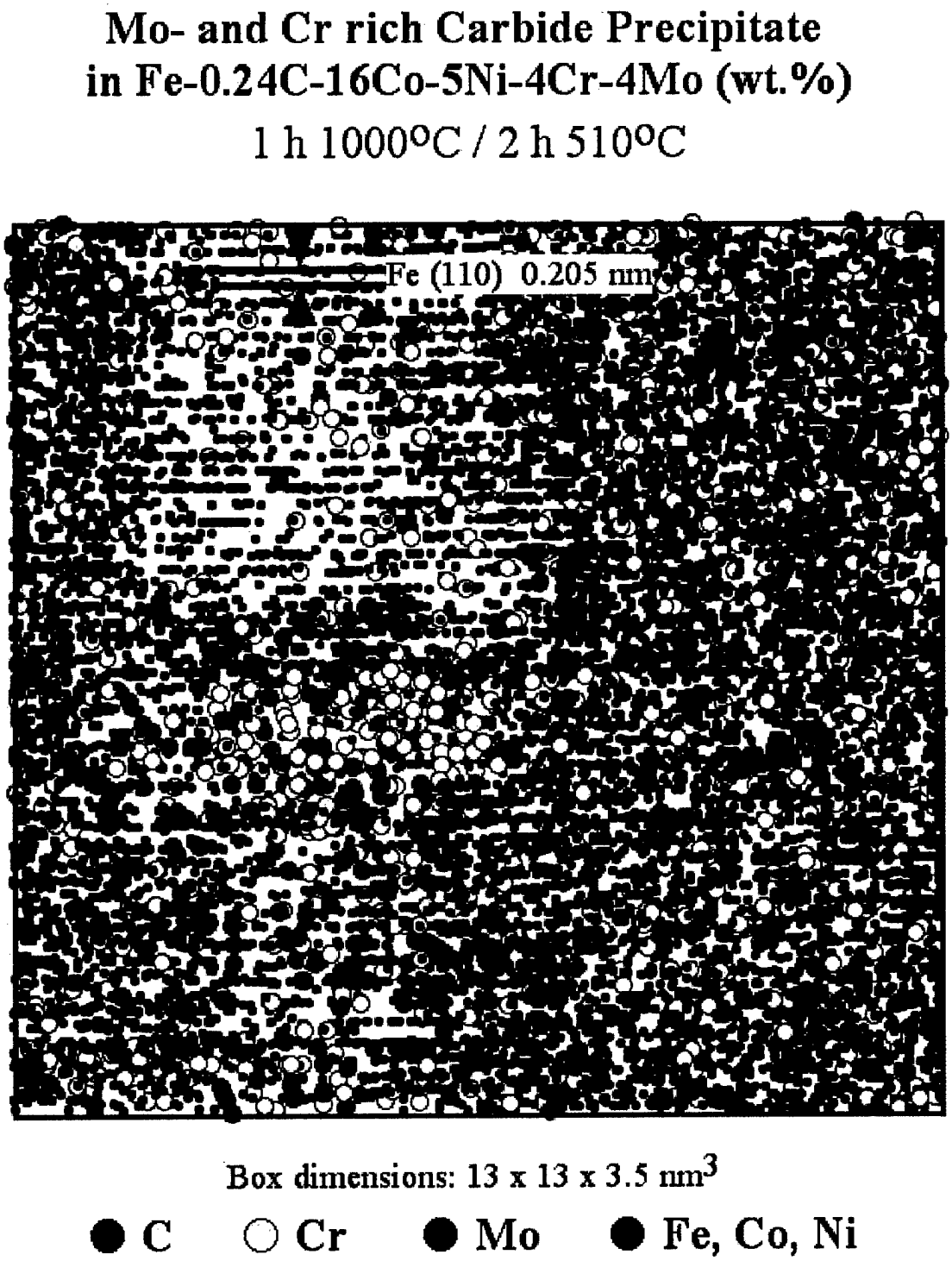

Figure 8. 3D Atom Probe reconstruction of M_2C carbide in 0.24C-16Co-5Ni-4Cr-4Mo steel solution treatment 1000 °C, 1hr, tempered 500 °C, 2hr to peak hardness of Rc 60.

2. Toughening

Early work under the SRG Program addressed toughening of UHS steels via (a) control of microvoid nucleating particle dispersions governing plastic shear localization [48-51], and (b) dispersed-phase transformation toughening by precipitation of optimal stability austenite particles [52,53]. A continuing effort under ONR support has defined requirements to resist intergranular fracture [54]. Guided by model predictions on microvoiding behavior, the doctoral research of C. J. Kuehmann under ARO support addressed optimization of the solution treatment of the commercial Aermet100 alloy to obtain a residual grain refining dispersion of fine TiC particles with improved resistance to microvoiding as attested by J_{IC} toughness measurements [55]. Kuehmann then explored optimization of multistep tempering treatments to achieve dispersed-phase transformation toughening in this alloy.

Our understanding of transformation toughening mechanisms benefited from a parallel DOE-sponsored effort studying fully austenitic alloys, experimentally demonstrating the role of phase stability and dilatation [2, 56-58] with numerical simulations defining the effect of transformation plasticity in enhanced resistance to plastic localization [59] and microvoiding processes [60]. ARO sponsored research has explored the application of this understanding to the control of dispersed-phase transformation plasticity in the secondary hardening martensitic steels. Our progress is summarized by the toughness-hardness plot in Figure 9. Early experiments guided by thermodynamic predictions of achievable austenite stability in the AF1410 composition boosted toughness to the AF1410-TT band employing multistep tempering to nucleate a fine dispersion of Ni enriched austenite while maintaining a sufficiently fine carbide dispersion for desired strength [52].

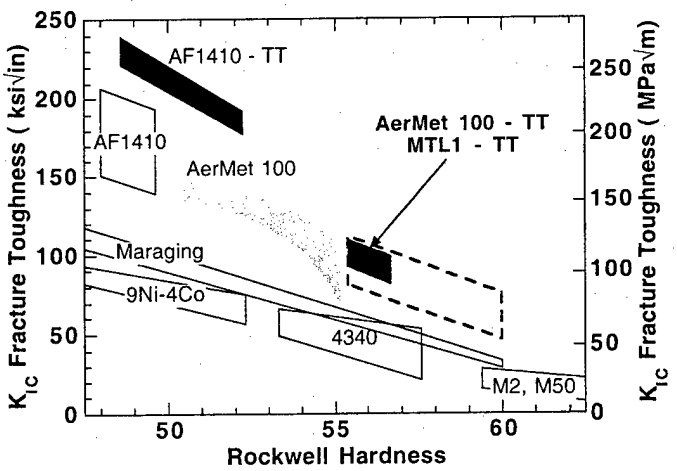

Figure 9. Toughness-hardness plot with dark bands denotes properties of transformation toughened (TT) materials; dashed box denotes original SRG objectives.

Our efforts to apply the same strategy to the higher strength Aermet100 alloy revealed a much tighter processing window due to the faster carbide precipitation kinetics associated with this higher Cr composition. Initial multistep tempering studies by Kuehmann [55] demonstrated transformation toughening, but at less than desired strength levels. A more thorough study was then undertaken by Visiting Scientist M. Srinivas from the Defence Metallurgical Research Laboratory, India, establishing first the detailed low temperature tempering kinetics for optimal strengthening, then interposing short intermediate temperature austenite nucleation treatments. Detailed measurement of toughness evolution was provided by relatively simple crack-tip stretch-zone measurements followed by verification of promising treatments with J_{IC} tests. The results of optimal processing are represented by the Aermet100-TT and MTL1-TT band in Figure 9. The outstanding toughness and hardness combinations are seen to lie within the dashed box representing the original property objectives of

the SRG program. Under a one-year contract from ARL/WMD (formerly MTL), SRG design tools were applied to the design of a prototype high hardness armor steel. This led to the alloy MTL1, which was evaluated by Kuehmann and J. Cho [55]. Employing a V addition to enhance strengthening efficiency, the alloy demonstrated properties equivalent to the Aermet100 alloy, but with lower C content (0.21C). Ballistic testing at ARL/WMD demonstrated V_{50} levels at fixed plate thickness equivalent to the best monolithic armor steels.

Austenite precipitation behavior in these alloys was then investigated by electron microscopy and microanalysis in the doctoral research of fellowship student H. Lippard [61] cosupervised by Prof. V. Dravid. Dark-field microscopy revealed two forms of precipitated austenite in the Aermet100-TT material. The microstructure is similar to our previous observations in AF1410-TT [52] in which slightly Ni enriched austenite discs at martensite lath boundaries coexist with a fine dispersion of more Ni rich intralath precipitates; the lath boundary precipitation gives nonequilibrium austenite compositions while the composition of the fine intralath precipitates is in reasonable agreement with equilibrium calculations. The high austenite stability responsible for toughening these UHS steels is attributed to the fine size and Ni enrichment of the latter. While the fine austenite in AF1410-TT had a particle size of 20nm, the fine particles observed in Aermet100-TT are only 5nm, taxing the limits of analytical electron microscopy. In addition to the 200 kV cold field emission Hitachi HF2000 analytical electron microscope at Northwestern, the samples were analyzed with a Phillips CM20 at Gatan Laboratories (employing a Gatan Imaging Filter for EELS imaging with the Ni core loss L-edge) and the highest brightness 300kV cold field emission UHV VG603 STEM at Lehigh University. The high resolution microanalysis quantified the fine particle compositions throughout the precipitation process, and revealed evidence of austenite nucleation on the Cr-rich carbides. Consistent with the carbide capillary energies defined by the analysis of Figure 5, Lippard extended the unstable equilibrium model to treat the trajectory of co-precipitation of austenite and M_2C. Figure 10 presents computed austenite Ni contents as a function of capillary energy in both austenite and M_2C. The boxes depict the trajectory of co-precipitation indicated by the austenite composition measurements. A greater than 50% drop in the M_2C capillary energy prior to austenite precipitation is consistent with austenite nucleation on the carbides.

While the analytical electron microscopy gives a plausible representation of co-precipitation, the new 3D atom-probe capability offers the opportunity for definitive measurement of both the austenite and associated carbides during austenite nucleation. A thorough investigation with this technique and an extension of the carbide precipitation computational model will allow full simulation of the co-precipitation of austenite and M_2C. Although the toughening results represented in Figure 9 demonstrate the potential of transformation toughening in these steels, the optimal austenite nucleation treatments in both AF1410-TT and Aermet100-TT required tempering times of 10 to 15 minutes, which would not be practical in many applications. A reliable, predictive co-precipitation model will be essential for the robust design of alloys capable of reproducibly achieving optimal transformation toughening with practical heat treatment conditions.

3. Gear Steels

Case hardenable secondary hardening steels for the high power density gear systems of Figure 2 may represent the most promising area for application of the design models we are developing. This line of research originated as conceptual designs in Materials Design class projects performed in collaboration with a mechanical engineering design class who identified property objectives for a 50% weight reduction in gears. Preliminary designs comparing low temperature nitriding and high temperature carburizing led to selection of carburizing as the most promising processing route to achieve the 1mm-scale case depths needed in typical gear applications. Two generations of carburizable prototype compositions were designed and evaluated. An undergraduate project evaluating the second prototype alloy, designated C2, won 1st prize in the TMS-AIME national student design competition [21].

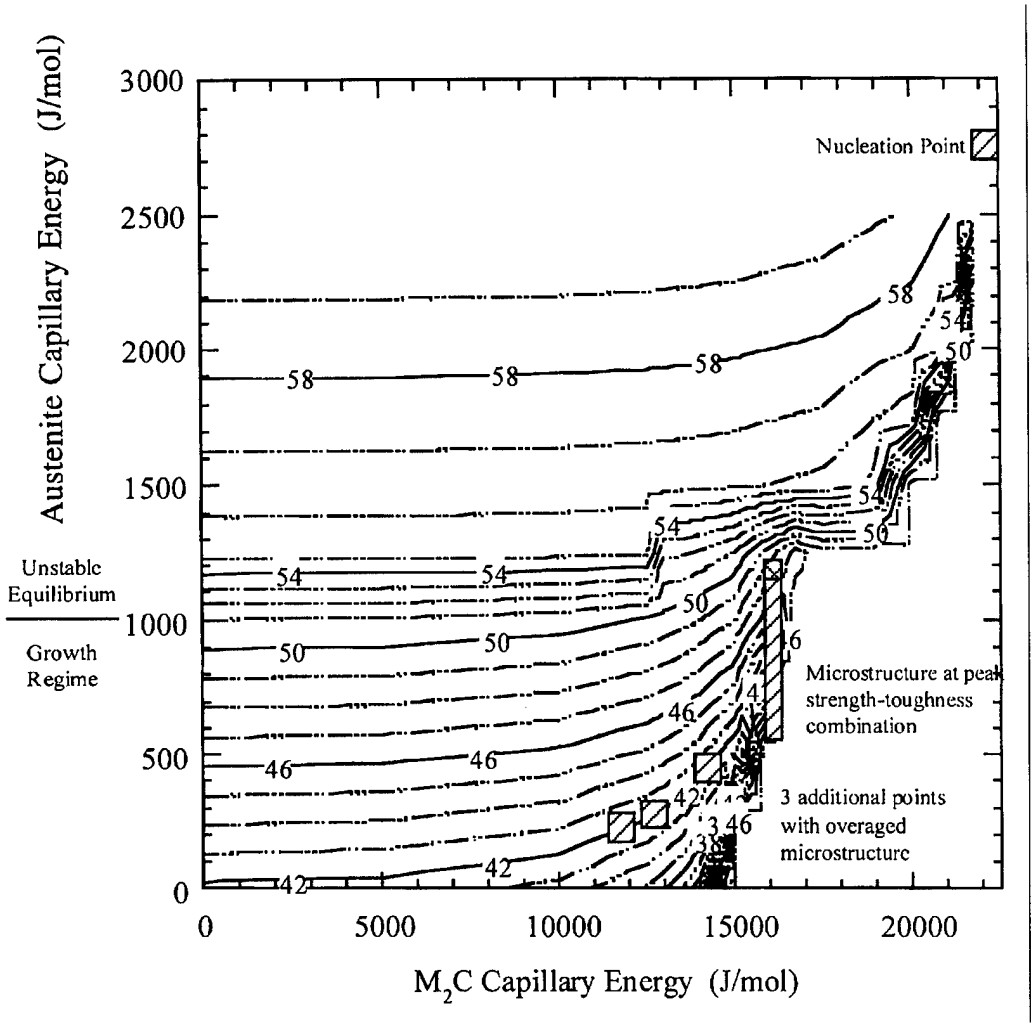

Figure 10. Contour plot of precipitated austenite Ni content (wt. pct.) for Aermet100 steel tempered at 455 °C, showing observed trajectory of austenite precipitation vs. M_2C and austenite capillary energy.

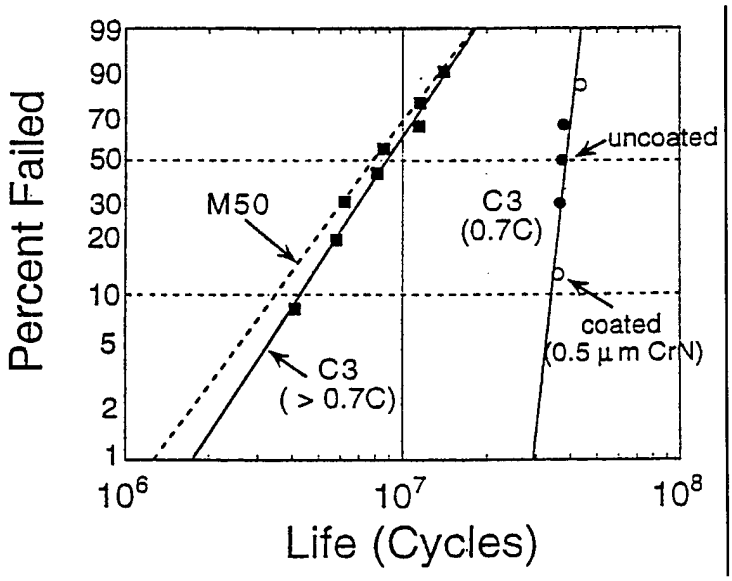

Figure 11. Probability distributions of RCF fatigue life in standard NTN ball-on-rod RCF tests comparing ultrahard case steels with M50 bearing steel.

Research on carburizable gradient systems for gear applications continued in the doctoral research of J. Wise[45,46], initiated under seed funding from the Ford Motor Company. Precise treatment of the dynamics of gradient formation by carburizing has been made possible by the DICTRA multicomponent diffusion code. To apply the code to carburization of the complex multicomponent steels of interest, Wise conducted preliminary carburizing experiments on an Fe20Co10Ni alloy and determined the composition-dependent C diffusivity from measured C profiles. Based on these measurements, it was found necessary to modify the DICTRA mobility database (mob4) through a Co-C interaction term. The model was then validated by comparison with measured diffusion profiles in carburized Aermet100 steel, demonstrating excellent agreement. Combining DICTRA diffusion simulations with the strengthening model of Figure 7 provides the basis for precise control of hardness profiles in these secondary hardening steels. The hardness profiles so far obtained in prototype gear steels compared with that of a conventional gear steel, demonstrate a case hardness increase of 50%. The corresponding increase in rolling contact fatigue (RCF) life obtained thus far is shown in Figure 11, based on the standard NTN ball-on-rod test. When carburized to case carbon content above the design level of 0.70C, fatigue life is comparable to the M50 bearing steel, and metallographic examination indicates fatigue initiation at large undissolved cementite particles. When the case is properly diffusion treated to the desired 0.70C level, these excess carbides are eliminated, and preliminary RCF data (with and without CrN coatings) indicates a narrower probability distribution with an order of magnitude life improvement over M50 at a 10% failure probability.

Research Assistant Jim Wright is continuing the RCF testing with a higher cleanliness heat of the experimental steels, and is investigating the nature of the microstructural instabilities causing "butterfly" and "white band" defects that precede RCF initiation in conventional gear and bearing steels. Wright is also performing X-ray diffraction studies to investigate the control of case residual stress in the new secondary hardening steels.

New developments in numerical applied mechanics methods provide a unique opportunity for fundamental modeling of the multiscale phenomena underlying the microstructural instabilities driving RCF initiation The multiple structural scales of concern are represented schematically in Figure 12. A typical contact width for a bearing is about 0.1 mm and contact stresses are significant over a depth (h) of about 1mm. The stresses induced by contact interact with subsurface inclusions which are about 2 microns in diameter. The material behavior on the submicron scale in the region of local stress concentrations associated with these inclusions is governed by the mechanisms of kinematic hardening and microvoid softening associated with 0.1μm scale second phase particles such as M_3C carbides.

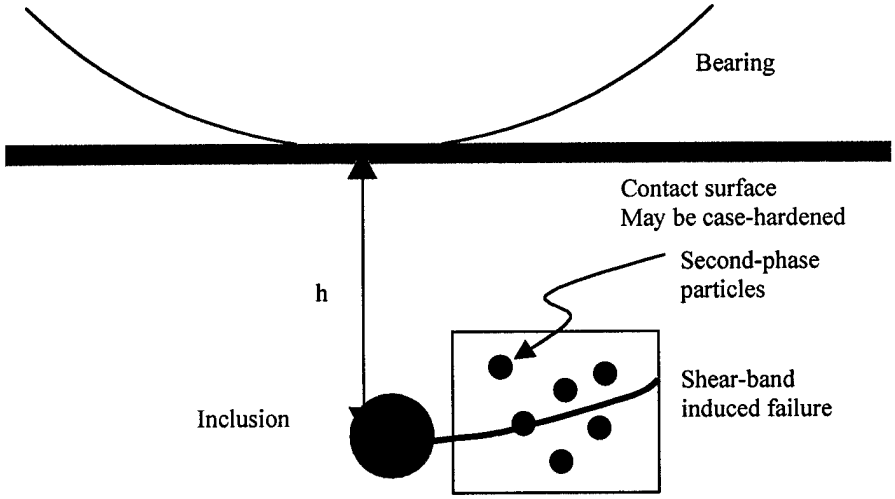

Figure 12. Multiple structural scales in RCF initiation represented for rolling element bearing.

The kinematic hardening is due to the Bauschinger effect associated with the back-stress induced by the second phase particles. This kind of behavior can be modeled using kinematic hardening plasticity models. Almer, Cohen and Moran [62] carried out finite element simulations of cyclic plasticity using a generalized plasticity model with kinematic hardening. The kinematic hardening was due to residual microstresses in ferrite induced by the inhomogeneous deformation fields around cementite particles. The finite element method was used to track the local stress-strain behavior in the vicinity of a stress concentration during a variety of press-fit operations. Almer et al. found good agreement between calculated residual stresses and those obtained by X-ray measurement techniques for dual phase materials. An interesting feature of this work is that the kinematic hardening parameter, for use in the constitutive model, was determined from X-ray measurements.

The microvoid softening is due to the nucleation and growth of microvoids at the second phase particles, which can ultimately lead to void-coalescence and the formation regions of strain localization or shear bands. This kind of behavior can be modeled by a Gurson type constitutive relation, which incorporates the nucleation and growth of voids.

4. Biomimetic Laminates

Testing the limits of complexity in rational materials design incorporating biomimetic adaptive system concepts, the essential concepts of the self healing "smart steel" superalloy composite are illustrated in Figure 13 and the flow block diagram, which summarized the concepts as a system chart, is shown in Figure 14. A ferritic (BCC) superalloy strengthened by a coherent dispersion of ordered B2 precipitates is reinforced by a thermodynamically compatible γ' strengthened austenitic (FCC) shape memory alloy in a laminate formed by hot rolling of a consolidated blend of prealloyed powders. The composite integrates two biomimetic concepts. At low temperatures the shape memory alloy reinforcement toughens the otherwise brittle ferritic alloy by bridging cracks via martensitic pseudoelasticity, mimicking the nonlinear polymer reinforcement of a brittle ceramic in the toughened laminate system of natural seashell [10,11]. Returning an internally damaged composite to the superalloy operating temperature, the bridges contract via the shape memory effect providing a crack clamping force to promote diffusional rewelding of cracks as a biomimetic self-healing mechanism. Thermodynamic compatibility demands that the BCC (α) and FCC (γ) alloys be in near-equilibrium with each other at hot working and solution treatment temperatures, and that the two 2-phase α+B2 and $\gamma+\gamma'$ alloys reside in an equilibrium 4-phase α+B2+$\gamma+\gamma'$ field at service temperatures. Matrix/reinforcement interfacial strength must be limited to promote crack bridging behavior, and the austenitic alloy must exhibit higher creep strength than the ferritic alloy to maintain crack clamping forces for damage healing.

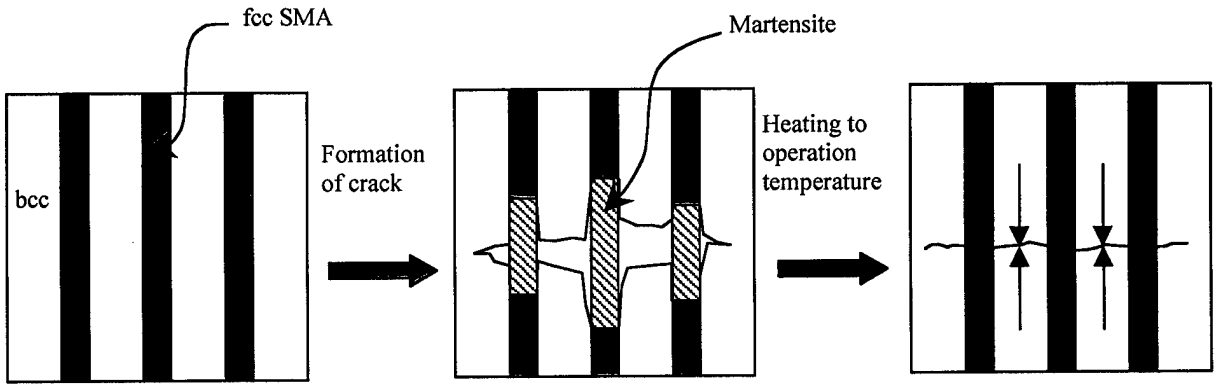

Figure 13. Schematic of biomimetic laminates. At low temperature, crack are formed, causing a thermoelastic martensite transformation in the reinforcement. Upon heating, the reverse martensitic transformation occurs, causing crack closure.

The original conceptual design and preliminary feasibility calculations by an undergraduate Materials Design class project team won 2nd prize in the first TMS-AIME national student design competition [20]. Under AASERT support, the doctoral research of Brad Files [63-66] explored the design of a precipitation-strengthened NiAl intermetallic reinforced by a thermodynamically compatible γ'-strengthened austenitic shape memory alloy. Thermodynamic models of the Fe-Ni-Al-Ti-Co-Mo system was refined with explicit treatment of order/disorder transitions underlying miscibility gaps. The models identified a suitable 4-phase α-B2-γ-γ' field at a service temperature of 600 °C in the basic Fe-Ni-Al-Ti system. Diffusion couples of alloys A and B, corresponding to α+B2 and γ+γ' alloys with dispersion fractions of 20% were prepared and reacted 24 hrs at 1100C to investigate the diffusional interaction at solution temperatures where each alloy should be single-phase. The electron microanalysis data (employing a Hitachi S-4500 FEG-SEM) demonstrated a sufficiently large diffusion distance of 50-100μm allowing accurate measurement of multicomponent diffusion composition trajectories. The measured trajectories were consistent with the predicted high Al diffusivity. The boundaries of the single phase fields at the respective Ti and Al contents of alloys A and B were calculated based on our database. These calculations indicated that alloy A was actually well within the two-phase α+γ field at 1100C. To simulate a couple between two single-phase alloys, DICTRA simulations were run modifying the alloy A composition to the nearby single-phase α composition. TEM microscopy revealed a martensitic structure in the alloy indicating the alloy was fully austenitic at 1100 °C. These preliminary couple experiments provided important input for refining the thermodynamic database to properly position the relatively narrow γ+α field in the region of interest, while also providing useful diffusivity information for further refinement of the DICTRA mobility database. The designed composite was fabricated as a laminate, demonstrating thermodynamic compatibility, crack-bridge toughening, and partial crack closure.

In a feasibility study, TiNi shape memory alloy wires were used as the reinforcement in a Sn-Bi matrix to attempt to show that a healing behavior can be mimicked in engineered structure materials. When the composite was pulled to 1% strain, 80% of the plastic deformation was returned by heating above the reversion temperature of the shape memory alloy fibers. In the case of a composite strained above 6%, surface macrocrack growth was stabilized by fiber reinforcement. Upon heating this sample close to the matrix melting point, fiber reversion provided crack closure and clamping, with an accompanying reversal of 2% strain [64]. A Freshman Design team (Terminator 3) then designed a Sn-Bi-In alloy matrix with controlled melting characteristics. As a Sophomore project, Priscilla Bernikowicz fabricated the designed composite, demonstrated the predicted crack healing by exploiting incipient melting, and won the 1998 TMS-AIME undergraduate paper competition [67]. A ternary Sn-based matrix alloy reinforced by TiNi shape memory alloy was shown to be capable of closing cracks and healing them when heated to a partially liquid state [68]. The roles of porosity, composite wire content, and phase fraction liquid during healing were assessed using metallography as well as the Thermo-Calc thermochemical software system. It was shown that a strength recovery of 88% was achieved in the cracked samples after healing. Following the TMS-AIME award winning work, the composition of the matrix alloy was further refined to increase the temperature range over which the alloy can be heated and a flux was designed to reduce oxidation of the sample and to increase the flow of the liquid alloy [69,70].

Over the past few years, several Terminator 3 prototypes have been developed by various student teams from the Engineering Design and Communications (EDC) program as well as from the MSc 390 Materials Design classes at Northwestern University. It has been demonstrated that this project is not too far away from bringing fiction to life. The concept of self-healing and "smart materials" has drawn attention of NASA-Houston, interested in having materials that can self-heal for remote repairing of space station parts. To make the alloy even smarter, a control system, or "brain" was designed to detect cracks and to command the heating procedure [71]. To accelerate the healing process the shape memory behavior of the TiNi alloy (Nitinol) was further investigated [72]. It was found that aging plays an important role in Ti-rich Nitinol wires. Ti_2Ni phase is usually found in the alloy, lowering the shape memory temperatures. Solution treatment can dissolve significant amount

of Ti_2Ni particles. Increasing the Ti content, the A_f temperature of the alloy (martensite to austenite transformation temperature) increases about 30 °C. The healing process is thus accelerated at the higher healing temperature. A complete crack healing was observed within 3 hours.

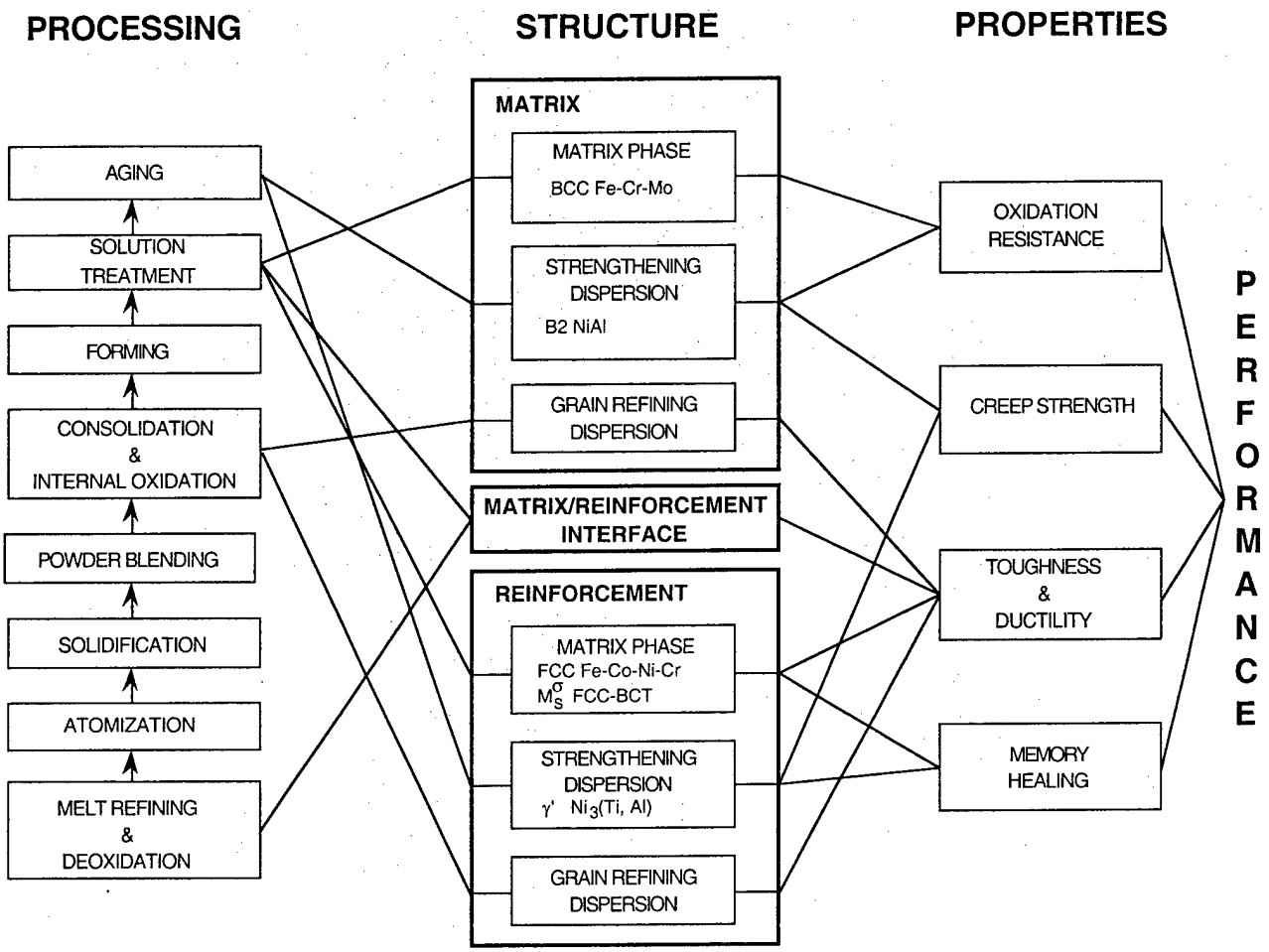

Figure 14. System structure of self-healing "smart steel" superalloy composite.

Under continuing AASERT support, doctoral student Deborah Burton, working with Prof. Moran, has implemented shape memory constitutive laws in a finite element simulation of such shape memory reinforced composites. The model will be applied to the prediction of optimal matrix and reinforcement characteristics for the extension of the healing concept to higher strength materials for application in smart structures.

Conceptual Designs: Metal/Ceramic Hybrid Armor

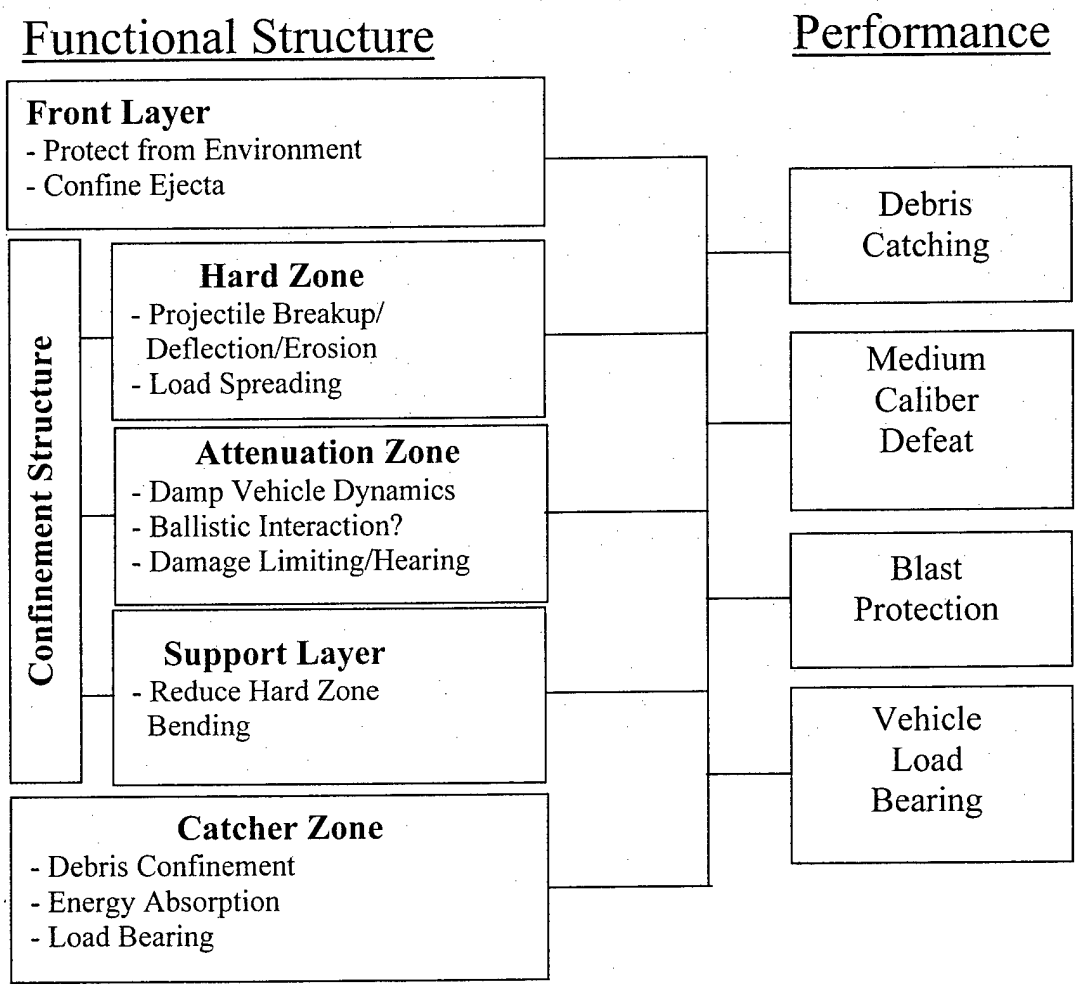

Figure 15. Multifunctional armor system block diagram.

A conceptual design activity led by Dr. Jian-Sheng Wang addressed various approaches to hybrid metal ceramic armor materials design beginning with the system block diagram of Figure 15 representing possible functions of the primary structural subsystems. One possible structural configuration considered in greatest detail is represented in Figure 16. In accordance with the requirements of figure 15, the system consists of 5 layers. The front layer is an organic coating for the protection of environment attact, confinement of ejecta and possibly others such as antiradar function etc. Our research has not assessed this layer in detail. The second layer is a hard layer for projectile breakup, deflection, erosion and load spreading. The requirements for this layer are: ultra high hardness combining with high toughness, constrained fracture and ability of crack arrest to limit impact damage and formation of debris, and capable of spreading impact load to reduce ballistic penetration. We propose a transformation-toughened UHS alloy grid with bonded CMC ply tiles as the hard layer. In order to reduce the vehicle weight, we explored the feasibility of transformation-toughened Ti-based alloys. The third layer is a possible nonlinear compliant material (rubberlike) for the damping of vehicle dynamics and absorption of ballistic impact energy. The fourth layer is a smart ceramic layer consisting of an SPPS ceramic matrix with Sn-based low melting-point particles and SMA reinforcement fibers. The SPPS ceramic matrix

provides ballistic penetration resistance. The SMA fibers provide bridging toughening under impact loading and crack closure and clamping effect during self-repairing. The Sn-based low melting-point particles provide self-healing for cracks. An acoustic sensor is attached to the layer to detect the damage. Whenever damage is detected, a high density low voltage DC current will be automatically activated through the SMA fibers heating up the Sn-based low melting-point particles providing self-healing of cracks. The fifth layer is a load bearing layer made of a case-hardened functional gradient UHS steel. This layer is also the substrate of the SPPS thick coating. The hardness varies gradually from the surface to the core. The high hardness surface provides further ballistic penetration resistance, the tough core provides load bearing, energy absorption and debris confinement. To restrict crack propagation, a laser local annealing technique could be applied to form a patterned soft network providing crack arrest function.

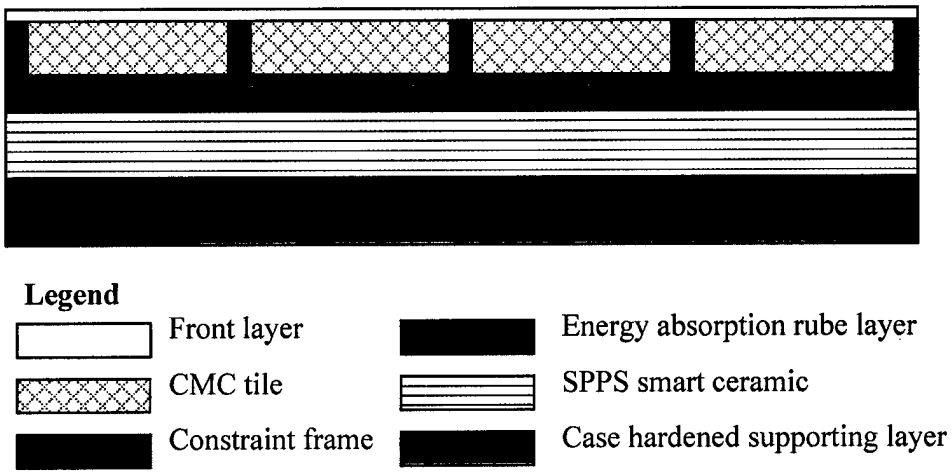

Figure 16. Schematic structure of an integrated multifunctional hybrid armor system.

1. The CMC ply tiles

An ultra high hardness is the primary requirement against ballistic penetration, this hard layer has to be ductile to resist debris formation. A single phased ceramic tile does not satisfy this requirement. The central technical problem for "toughened" materials is their lack of ductility and the associated scale dependence caused by weakest link dominance and the extreme value nature of the stochastic behavior. The weakest link scaling can be suppressed by imparting damage tolerance to the material, through mechanisms that stabilize sub-critical cracks. For this purpose, we propose CMC cross-plies as the anti-ballistic tiles. The advantage of the CMC cross-ply is that it provides toughness by the mechanisms of fiber pullout and crack deflection while maintaining the high hardness of the ceramic. We propose a 90 degree fiber reinforced CMC ply. The toughening effect induced by inelastic strains has been documented [73-76] and schematically shown in Figure 17 [77]. Upon tensile loading, cracks form in the 90° plies by tunneling with associated inelastic strain (Figure 17). Upon subsequent loading, as the cracks penetrate the 0° plies, they interact with the fibers and the coating. When debonding and slip occurs within the coating, two stresses characterize the inelastic strain: a friction stress τ, and a debond stress σ_i (Figure 17). The latter is related to the debond toughness for the coating and the residual stress. The consequent inelastic tensile strain depends on the stress acting on the 0° plies.

We propose TiB_2 as the matrix of the CMC plies. A comparison of thermomechanical properties of various ceramics, including oxides, carbides and borides, is shown in Table 2. TiB_2 shows the best combination of the ultra high hardness with good toughness. The hardness of TiB_2 is less than diamond and cubic BN, ranking as the third hardest material in nature. Considering the primary candidate materials of the confinement grid, Ti-based alloys, there are other advantages of choosing TiB_2 as the matrix material: the crystallographic structure, the density, and the coefficient of thermal expansion (CTE) of TiB_2 are comparable with Ti-based alloys. It is expected that the residual stress at the CMC/Ti interface is low, and the bonding between them is strong, inducing large confinement due to crack arrest and load spreading.

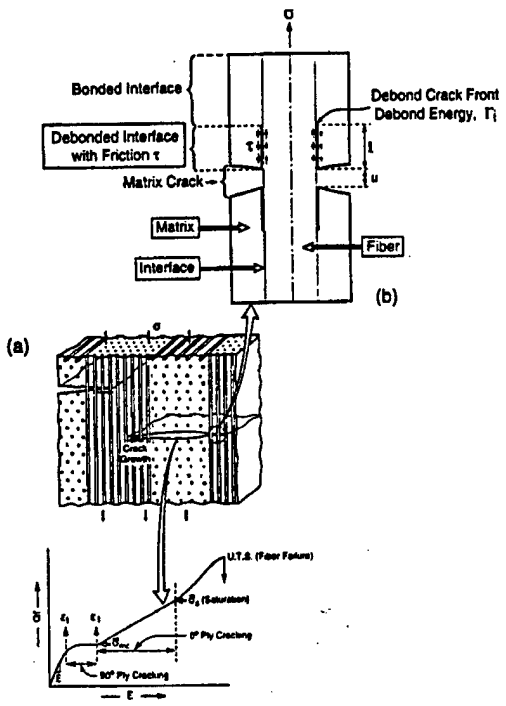

Figure 17. The ply cracking model and the associated stress-strain curve (a) and the cell model for inelastic strains in the 0° plies.

Commercially available ceramic fibers are limited to Nicalon and Tyralon, which are SiC-based fibers. SiC-matrix CMCs with Nicalon or Tyralon reinforcement fibers and BN coatings has been extensively studied. We propose use of these commercial fibers in our TiB_2 matrix CMC. We next need to investigate the compatibility between the fiber and the matrix, the thermomechanical behaviors of the CMC, the processing and the anti-ballistic performance of the CMC tile.

2. Constraint Frame

We propose transformation-toughened UHS steels and Ti-base alloys as the constraint grid materials to provide constraint for crack propagation in the CMC tiles and preventing debris. Our understanding of dispersed-phase transformation toughening mechanisms has been summarized earlier. Plastic deformation causes retained austenite particles to transform to martensite inducing a delayed hardening effect and enhanced resistance to plastic localization. ARO sponsored research has explored the application of this understanding to the control of dispersed-phase transformation plasticity in the secondary hardening martensitic steels. Outstanding toughness and hardness combinations have been achieved in Aermet100-TT and MTL1-TT steels.

Table 2:

Material	Crystal	d g/cm^3	Hardness GPa	K_{IC} $MPa\,m^{1/2}$	E GPa	ν	α $10^{-6}/K$	κ W/m K
Al_2O_3	Hexagonal	3.97	23	2.7-4.2	380	0.26	7.2-8.6	27.2
YSZ	Partial Cubic	5.7	11	6-9	205	0.23	8.9	1.8-2.2
ZrO_2	Cubic	5.56	15	2.8	207	0.23	13.5	1.7-1.9
TiB_2	Hexagonal	4.5	45	6-8	537	0.093	8.1	65-120
B_4C	Hexagonal	2.51	30		410		5	35
TiC	Cubic	4.92	35	1.7-3.0	430	0.19	7.4-8.6	33-43
SiC	α– Hexagonal	3.21	30	2.6-5.0	450	0.17	4.3-5.6	63-155
Si_3N_4	α– Hexagonal	3.18	9	3.6-6.0	304	0.24	3.0	9-30
TiN	Cubic	5.43	20	3.4-5.5	475	0.25	8.0	24
BN	Cubic	3.48	65	5.0	923	0.115	12.2	240

The same principles for UHS steels can be applied for the investigation of phase-transformation toughening Ti-based alloys. The choice of Ti-based alloy as the constraint grid material can reduce the weight of the vehicle and improve the compatibility between the grid material and the CMC tiles. We propose design of a phase-transformation toughening UHS Ti-based alloy. Ti-based alloys can undergo martensitic transformation the same as in steels. THERMOCALC/DICTRA modeling can explore the feasibility of developing a Ti-based alloy with retained "austenite" particles,. addressing precipitation hardening, the stability of the retained austenite and the kinetics of the stress induced martensite transformation in the alloy.

3. The smart material

We propose a smart ceramic composite thick coating consisting of an SPPS ceramic matrix with shape memory alloy (SMA) reinforcement fibers. The composite integrates two biomimetic concepts: at room temperature the shape memory alloy reinforcement toughens the ceramic by bridging cracks via martensitic pseudoelasticity, mimicking the nonlinear polymer reinforcement of a brittle ceramic in the toughened laminate system of natural seashell. At an elevated temperature, the bridges contract via the shape memory effect providing a crack clamping force. To promote diffusional rewelding of cracks as a biomimetic self-healing mechanism low melting-point Sn-based alloy particles can be co-deposited by SPPS processing. To make the ceramic even smarter, a sensor for detecting cracks and an actuator for initiating heating of the ceramic can be attached. Whenever damage of the system is detected, a high density, low voltage DC current can be automatically activated through the SMA fibers heating up the Sn-based low melting-point particles providing self-healing of cracks.

The matrix of the smart ceramic composite we proposed is partially stabilized ZrO_2 (YSZ). YSZ thick coating can co-deposit with a self-healing Sn-based alloy by SPPS process. Reinforcement fibers of TiNi SMA (Nitinol) can be added during deposition. YSZ has the highest toughness among the ceramics listed in Table 2. The comparable elastic modulus of YSZ with that of SMA insures a easy crack closure by contraction of the SMA fibers. The extremely low thermal conductivity of YSZ insures efficient heating up of the smart ceramic for self-healing. The thermodynamic compatibility between the components must be addressed along with the thermomechanical properties, the bridging toughening effect and the self-healing behavior of the smart ceramic. With an acoustic device attached to the system, one can study the sensibility of the acoustic emission in determining the crack density and determine the critical value of the acoustic signal under the pre-determined damage tolerance. The critical signal can be sent out to actuate a switch to allow a low voltage-high density current passing through SMA fibers heating up the composite to the A_1 temperature of the SMA. At this temperature, reverse phase transformation occurs in the deformed SMA and the SMA fibers return to the undeformed shape inducing crack closure of the damaged composite. To insure rewelding of the crack surfaces, particles of a low melting point alloy are co-deposited with YSZ by SPPS processing. The melting point of the alloy should be slightly lower than the A_1 temperature of the SMA. The alloy must have a good wetability with YSZ and a low viscosity at the liquid state. The Terminator 3 project can continue to design the Sn-Bi-In alloy. The composition of the alloy, the roles of porosity and fiber content of the composite need be assessed using metallography and the THERMOCALC/DICTRA software system.

4. Strengthening of a functionally graded case hardened steel

We propose a case-hardened functional gradient UHS steel as the load bearing layer of the armor system. The hard surface provides further ballistic penetration resistance, the tough core provides load bearing, energy absorption and debris confinement. To restrict crack propagation in the hard layer, a laser local annealing technique can be applied to form a patterned soft network providing crack arrest function. This load bearing layer is coated with the smart ceramic coating.

High temperature carburizing has been shown the most promising processing route to achieve about 1 mm-scale case depths needed. Employing a V addition to enhance strengthening efficiency, the MTL1 alloy has demonstrated properties equivalent to the Aermet100 alloy, but with lower C content (0.21C). Ballistic testing at ARL/MD demonstrated V_{50} levels at fixed plate thickness equivalent to the best monolithic armor steels. A higher carbon composition (0.25C) may further increase the hardness. This prototype alloy may be too costly, however, for applications in the armor system. A new alloy with less content of Co and Ni can be designed by THERMOCALC computations. Co could be replaced by Al, and Ni can be partially replaced by Mn. The THERMOCALC/ DICTRA code can be used to design carburization of the new complex multicomponent steels. Combining DICTRA diffusion simulations with the strengthening model provides the basis for precise control of hardness profiles in these secondary hardening steels.

Exploration of Shearable Matrix Alloys for Tungsten Heavy Alloy Penetrators

Based on the premise that the shearability of U penetrator alloys is based on the transformation plasticity associated with adiabatic transformation to the softer bcc phase, the Senior Project of Andrew Elliott, aided by thermodynamic modeling of Dr. Gautam Ghosh, addressed design of Hf-Ta-based alloys with identical transformation characteristics, for application as matrix alloys for shearable WHA penetrators. After thermodynamic assessment of the Hf-Ta binary system, button alloys were prepared by both elemental powder sintering and remelting. Although transformation temperatures could not be clearly measured, alloy hardness levels of 330 VHN were obtained with desired martensitic microstructures. Tests at ARL have shown that Hf-Ta alloys demonstrate desired adiabatic shear behavior. A marked copy of Elliott's report is attached as appendix B.

Bibliography

(* denotes references acknowledging ARO support)

1. C. S. Smith, A Search for Structure, (1981) MIT Press: Cambridge MA
2*. G.B. Olson, "Science of Steel", in Innovations in Ultrahigh-Strength Steel Technology, ed. G.B. Olson, M. Azrin, and E.S. Wright, Sagamore Army Materials Research Conference Proceedings: 34th (1990) 3-66.
3*. G.B. Olson, "Materials Design: An Undergraduate Course," Morris E. Fine Symposium, eds. P.K. Liaw, J.R. Weertman, H.L. Markus, and J.S. Santner, TMS-AIME Warrendale, PA (1991) pp. 41-48.
4. C. J. Kuehmann and G. B. Olson, "Computer-Aided Systems Design of Advanced Steels," Proc. International Symposium of Phase Transformations During the Thermal/Mechanical Processing of Steel - Honoring Professor Jack Kirkaldy, E. B. Hawbolt et al., eds., Metallurgical Society of the Canadian Institute of Mining, Metallurlgy and Petroleum, Vancouver BC (1995) 345-356.
5. T. A. Stephenson, C. E. Campbell, and G. B. Olson, "Systems Design of Advanced Bearing Steels," in Advanced Earth-to-Orbit Propulsion Technology 1992, eds. R. J. Richmond and S. T. Wu, NASA Conf. Pub. 3174, Vol II (1992) pp. 299-307.
6. B. Sundman, B. Jansson and J. O. Andersson, "THERMOCALC: a Thermochemical Databank and Software System," *CALPHAD* **9** (1985) 153.
7. G. B. Olson, Materials Design Initiative, Dept. Materials Science and Engineering, Northwestern University, Evanston, IL.
8. C. S. Smith, "A History of Martensite: Early Ideas on the Structure of Steel," in Martensite, eds. G. B. Olson and W. S. Owen, ASM: Materials Park, OH (1992) pp. 11-20.
9. G. B. Olson and H. Hartman, "Martensite and Life: Displacive Transformations as Biological Processes," *J. de Physique* **43** (1982) C4-855.
10. M. Sarikaya and I. A. Aksay, "An Introduction to Biomimetics: A Structural Viewpoint," *J. Mater. Sci.* (1993).
11. M. Sarikaya and I. A. Aksay, "Nacre of Abalone Shell: a Natural Multifunctional Nanolaminated Ceramic-Polymer Composite Material," in Results and Problems in Cell Differentiation, ed. S. T. Case, Springer-Verlag: Berlin (1992) pp. 1-26.
12*. G. B. Olson, M. Azrin and E. S. Wright, eds. *Innovations in Ultrahigh-Strength Steel Technology*, Sagamore Army Materials Research Conf. Proc.: 34th (1990).
13*. G. B. Olson, "Computational Design of Hierarchically Structured Materials," *Science* Vol. 227 (1997) pp. 1169-1404.
13a. G. B. Olson, "Designing a New Material World," *Science* Vol. 288 (2000) pp. 993-998.
14. J. B. Cohen and G. B. Olson, organizers, "Materials by Design," Gordon Research Conference, August 1993.
14a. G. B. Olson, "Computational Design of Hierarchically Structured Materials," to appear in *Proc. ISAEM-2000: 2nd International Symposium on Designing, Processing and Properties of Advanced Engineering Materials*, October 20-21, 2000, Guilin, P.R. China.
15*. G. B. Olson, "Systems Design of Hierarchically Structured Materials: Advanced Steels," *J. Computer-Aided Mat. Des.***4** (1997) pp.143-156.
16*. G. B. Olson, "Materials Design: Building a Better Martensite," *Proc. Intl. Conf. Displacive Phase Transformations and Their Applications in Materials Engineering*, TMS-AIME, 1996, pp. 15-26.
17*. G. B. Olson and C. J. Kuehmann, "Materials Design: Weld Metals for Elevated Temperature Service," *Mathematical Modelling of Weld Phenomena 4*, Proc. 4th Intl. Seminar on Numerical Analysis of Weldability, IOM Communications Ltd., London, 1998, pp. 290-301.
18. C. J. Kuehmann and G. B. Olson, "Gear Steels Designed by Computer," *Adv. Mat. & Proc.*, Vol. **153**, No. 5 (1998) pp. 40-43.

19. I. Amato, "What's cooking in the chem labs?" Fortune, Industrial Management & Technology edition, Apr. 17, 2000, pp. 454[C-W].
20. E. Chu, D. Fong, C. Klapperich and T. Yeh, Terminator 3: Biomimetic Smart Steels, MSc C90 Materials Design project report, June 1993, Northwestern University; 2nd prize, TMS-AIME MaD93 student design competition.
21. D. J. Cook and G. A. Lewis, High Performance Secondary Hardening Gear Steel Design and Evaluation, June 1994, Northwestern University; 1st prize, TMS-AIME MaD94 student design competition.
22. B. Forbes, Lower-Cost Secondary Hardening Steels, June 1994, Northwestern University; 2nd prize, TMS-AIME MaD94 student design competition.
23. A. Rentschler, Northwestern University, Composite Design, 2nd prize, TMS-AIME MaD96 student design competition.
24. "Miracles by Design", *Infinite Voyage* Special, PBS-TV; educational Discovery Lecture, NTU-TV, February 13, 1991.
25. "The New Alchemy", *Business Week*, July 29, 1991.
26. *Time* International Edition, Special "Discovery" Issue, Winter 1997-98.
27. I. Amato, "A Faster Track to Better Steels," *Fortune*, Industrial Management & Technology edition, March 2, 1998, 174[C-L].
28. I. Amato, *Stuff*; Basic Books, 1997.
29*. H. E. Lippard, C. E. Campbell, T. Bjorklind, U. Borggren, P. Kellgren, V. P. Dravid, and G. B. Olson, "Microsegregation Behavior During Solidification and Homogenization of AerMetlOO® Steel," *Met. Trans B,* 29B (1998) pp. 205-210.
30. G. R. Speich, "Secondary Hardening Ultrahigh-Strength Steel," *in Innovations in Ultrahigh Strength Steel Technology*, eds. G. B. Olson, M. Azrin and E. S. Wright, Sagamore Army Materials Research Conf. Proc.: 34th (1990) pp. 89-112.
31*. J. S. Montgomery and G. B. Olson, "M2C Carbide precipitation in AF1410," in *Gilbert R. Speich Symp. Proc.: Fundamentals of Aging and Tempering in Bainitic and Martensitic Steel Products*, eds. G. Krauss and P. E. Repas, ISS-AIME: Warrendale, PA (1992) pp. 177-214.
32. A. J. Allen, D. Gavillet and J. R. Weertman, "SANS and TEM Studies of Isothermal M2C Carbide Precipitation in Ultrahigh Strength AF1410 Steels," *Acta Metall.* **41** (1993) 1869.
33. J. S. Langer and A. J. Schwartz, *Phys. Rev.* **A21** (1980) 948.
34. R. Wagner and R. Kampmann, "Solid State Precipitation at High Supersaturations," in *Innovations in Ultrahigh Strength Steel Technology*, eds. G. B. Olson, M. Azrin and E. S. Wright, Sagamore Army Materials Research Conf. Proc.: 34th (1990) pp. 209-222.
35*. A. Umantsev and G. B. Olson, "Ostwald Ripening in Multicomponent Alloys," *Scripta Metall.* **29** (1993) 1135-1140.
36*. K. C. King, G. B. Olson and T. Mura, "Elastic Energy of Coherent Precipitation at Dislocations in an Anisotropic Matrix," *Proc. ARO Workshop, Modern Theory of Anisotropic Elasticity and Applications*, Ed. J. J. Wu, T. C. T. Ting, and D. M. Barnett, SIAM: Philadelphia, PA (1991) pp. 103-121.
37*. C. J. Kuehmann and P. W. Voorhees, "Ostwald Ripening in Ternary Alloys," Met. Trans. A, **27A**, (1996), 937-943.
38*. A. Umantsev and G. B. Olson, "Ostwald Ripening in Multicomponent Alloys," *Scripta Metall.* **29** (1993) 1135-1140.
39. C. A. Knepfler, "Synthesis and Characterization of Molybdenum-Based M2C Carbides," Ph.D. thesis, Northwestern University Dept. Materials Science and Engineering, December, 1994.
40*. C. A. Knepfler, K. T. Faber, J. Weertman, G. B. Olson, C. R. Hubbard, O. B. Cavin and N. Packen, "High Temperature Stability and Thermal Expansion Behavior of Molybdenum-Chromium M2C Carbides," *J Alloys & Compounds* **248** (1997) 139-142.

41. R-H. Liarng, "Application of the Eigenstrain Method in Inclusion Problems And Micromechanics of Coherent M2C Carbide Precipitation in Steel," Doctoral Thesis, Northwestern University, Dept. Civil Engineering, December, 1996.
42*. Y. Nagataki, J. B. Cohen and G. B. Olson, "Xray Line Broadening Study of M_2C Precipitation in Co-Ni Secondary Hardening Steels," to appear in *Proc. Advanced Materials for the 21st Century: The Julia R. Weertman Symposium*, MRS.
43. C. E. Campbell, "Systems Design of High Performance Stainless Steels," Doctoral Thesis, Northwestern University, Dept. of Materials Science and Engineering, June, 1997.
44. C. E. Campbell and G. B. Olson, "Systems Design of High Performance Stainless Steels I. Conceptual Design; II. Prototype Evaluation," submitted to *J. Computer-Aided Design*.
45. J. Wise, "Systems Design of Advanced Gear Steels," Doctoral Thesis, Northwestern University, Dept. of Materials Science and Engineering, June, 1998.
46. C. J. Kuehmann, J. P. Wise, C. E. Campbell and G. B. Olson, "Simulation of Carburization in Secondary Hardening Steels," *Proc. Heat Treat '97*, ASM Intl., Materials Park OH, 1997.
47. G. Ghosh, C. E. Campbell and G. B. Olson, "An Analytical Electron Microscopy Study of Paraequilibrium Cementite Precipitation in Ultra-High-Strength Steel," *Metall. Mater. Trans.* **30A** (1999) 501-512.
48. A. Needleman, "A Numerical Study of Void Nucleation at Carbides," in *Innovations in Ultrahigh-Strength Steel Technology*, G. B. Olson, M. Azrin and E. S. Wright, eds., Sagamore Army Materials Research Conf. Proc.: 34th (1990) p. 331.
49. J. W. Hutchinson and V. Tvergaard, "Effect of Particle-Void Interaction on Void Growth in Tension and Shear," in *Innovations in Ultrahigh-Strength Steel Technology*, G. B. Olson, M. Azrin and E. S. Wright, eds., Sagamore Army Materials Research Conf. Proc.: 34th (1990) p. 347.
50. J. G. Cowie, M. Azrin and G. B. Olson, "Microvoid Formation During Shear Deformation of Ultrahigh-Strength Steels," *Metall. Trans. A.* **20A** (1989) 143.
51. M. J. Gore, G. B. Olson and M. Cohen, "Grain-Refining Dispersions and Properties in Ultrahigh-Strength Steels," in *Innovations in Ultrahigh Strength Steel Technology*, eds. G. B. Olson, M. Azrin and E. S. Wright, Sagamore Army Materials Research Conf. Proc.: 34th (1990) pp. 425-442.
52. G. N. Haidemenopoulos, G. B. Olson, and M. Cohen, "Dispersed-Phase Transformation Toughening in Ultrahigh-Strength Steels," in *Innovations in Ultrahigh Strength Steel Technology*, eds. G. B. Olson, M. Azrin and E. S. Wright, Sagamore Army Materials Research Conf. Proc.: 34th (1990) pp. 549-596.
53. G. N. Haidemenopoulos, G.B. Olson, M. Cohen, and K. Tsuzaki, "Transformation Plasticity of Retained Austenite in Stage I Tempered Martensitic Steels, "*Scripta Metall.* **23** (1989) 207-211.
54. D. Spaulding, G. B. Olson and Y-W. Chung, "Grain Boundary Cohesion and Segregation in Ultrahigh Strength Steels," submitted to *Metall. Mater. Trans. A*.
55*. C. J. Kuehmann, J. Cho, T. A. Stephenson, and G. B. Olson, "Systems Design of High Performance Steels," *Metallic Materials for Lightweight Applications* (40th Sagamore Army Materials Research Conference), eds. E. B. Kula and M. G. H. Wells, U.S. Government Printing Office, Washington, DC, Lake George, NY (1994) 337-355.
56. C-C. Young, "Transformation Toughening in Phosphocarbide-Strengthened Austenitic Steels," Ph.D. Thesis, MIT Dept. Materials Science and Engineering, June 1988.
57. F. Stavehaug, "Transformation Toughening of γ' Strengthened Metastable Austenite Steels," Ph.D. Thesis, MIT Dept. Materials Science and Engineering, June, 1990.
58. D. Bergstrom, "Transformation Toughening in UHS Austenitic Steels," Ph.D. thesis, Northwestern University Dept. of Materials Science and Engineering, June, 1996.
59. R. G. Stringfellow and D. M. Parks, "Strain-Induced Transformation Toughening in Metastable Austenitic Steels," in *Fracture Behavior and Design of Materials and Structures, Vol. 1*, Ed. D. Firrao, EMAS Ltd., Warley, U.K., 1992, p. 400.
60. S. Socrate, "Mechanics of Microvoid Nucleation and Growth in High Strength Metastable Austenitic Steels", Ph.D. thesis, MIT, March, 1995.

61. H. Lippard, "Microanalytical Investigations of Transformation Toughened Co-Ni Steels," Ph.D. thesis, Northwestern University Dept. of Materials Science and Engineering, December 1999.
62. Almer, J. Cohen, J. B. and Moran, B. "The Effects of Residual Stresses on Fatigue Crack Initiation", manuscript in preparation.
63. B. Files, "Design of a Biomimetic Self-Healing Superalloy Composite," Doctoral Thesis, Northwestern University, Dept. of Materials Science and Engineering, December, 1997,
64*. B. Files and G. B. Olson, "Terminator 3: Biomimetic Self-Healing Alloy Composite," *SMST-97: Proc. 2nd Intl. Conf. Shape Memory & Superelastic Technologies*, SMST, Santa Clara CA, 1997, pp. 281-286.
65.* G. B. Olson, "Systems Design of Hierarchically Structured Materials: Smart Steels," *Proc. Intl. Forum on Creation of Super Metallic Materials Consisting of Amorphous, Nanoscale and Mesoscopic Structures*, R&D Institute of Metals and Composites for Future Industries (RIMCOF), Tokyo, Feb. 7, 1997.
66*. G. B. Olson, "Brains of Steel: Designing Materiallurgists," *Adv. Mat. & Proc.* Vol. **152**, No. 1 (1997) pp. 72-79.
67*. P. Bernikowicz, "Terminator III: Design of Tin-Based Biomimetic Self-Healing Alloy Tensile Specimens," TMS-AIME 1998 Undergraduate Paper Competition.
68. C. Forbell, M. Barney, C, Scharff and W. Lai, "Tin Based Sefl-Healing Alloy", MSc C90 Materials Design project report, Northwestern University, June, 1995.
69. E. Tao, M. Price, J. Asahara, K. Benes and T. Key, Terminator 3: Creating a Metal that Mimics Biological Healing, Freshman Design project report, Northwestern University, June, 1998.
70. J. Hughs and D. Relles, Healing in Terminator 3: Advancements in a Biomimitic Sefl-Healing Superalloy Composite, MSc C90 Materials Design project report, Northwestern University, June, 1998.
71. E. Heneghan, D. Lee, B. Pasquini and P. Pavi-Shankar, Terminator 3, Freshman Design project report, Northwestern University, June, 1999.
72. B. Lohwongwatana, Terminator 3; Design of High-Temperature Biomimetic Self-Healing Alloy Composites, C96 Senior Project report, Northwestern University, June, 2000.

PATHWAYS OF DISCOVERY

Designing a New Material World

Gregory B. Olson

Materials have paced the evolution of technology for millennia. Their importance in the advance of human civilization is apparent in the naming of historical epochs, from the Stone Age through the Bronze and Iron Ages and into the ongoing Silicon Age. The origin of diversity in the material world remains largely mysterious to the public, yet the specialists' ability to understand and manipulate the microstructures of materials has grown explosively over the past half-century. As the new millennium unfolds, a confluence of natural philosophies—one that combines reductionist and synthetic thinking—is ushering in an Age of Design marked by new materials and ways of creating them that go beyond the dreams of the medieval alchemists.

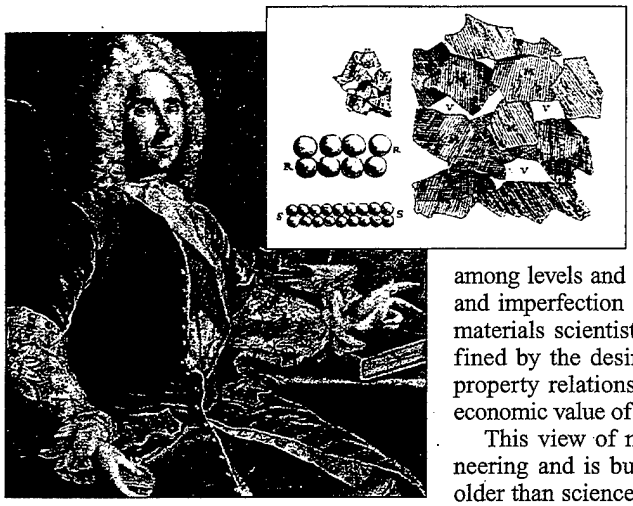

Materials savant. René de Réaumur and his 1722 sketch of steel's anatomy.

Materials as Systems

The modern view of materials structure was best expressed by the late philosopher-scientist Cyril Stanley Smith *(1)*. He described a universal multilevel nature of structure with strong interactions among levels and an inevitable interplay of perfection and imperfection at all levels. Smith argued that the materials scientist's distinct view of structure is defined by the desire to understand the structure and property relations underlying the technological and economic value of materials.

This view of matter integrates science and engineering and is built on a natural philosophy that is older than science. Smith identifies the origin of this philosophy within medieval alchemy, whose practitioners are mostly remembered for their attempts to "transmute" base metals into gold. They knew nothing about protons and electrons. Still, Smith asserts that their aspirations, motivations, and even concepts resembled the modern materials engineer's use of complex processing to "transmute" the multilevel microstructure of materials (from the atomic to macroscopic levels) to achieve the essential property of gold, namely, economic value.

The property-driven view of structure and processing for the creation of value, shared by modern materials science and alchemy, embraces an essential complexity of material structure. During the 17th century birth of modern science, Smith identifies a short-lived Golden Age of materials science under the leadership of René Descartes, whose "corpuscular" philosophy inspired the development of a multilevel view of structure to account for the diverse properties of materials.

The prescient grasp of materials achieved by the corpuscularians is well represented by René Antoine Ferchault de Réaumur's 1722 sketch of the structure of quench-hardened steel (see figure above). He proposed that a single grain of steel (G), if enlarged, would reveal a set of "molecules" (M) and voids (v). Higher magnification would reveal a substructure of the molecules (pp); and yet higher magnification would show an aperiodic arrangement of spheres. The finest scale Réaumur envisioned corresponds to a periodic packing of spheres, what we might think of as the nanoscale.

This elegant view contained many structural elements of modern materials science. There was no instrumentation with which to validate it, however, so the complex structural view was supplanted by more intellectually compelling but overly simplistic notions. One was Isaac Newton's continuum, which erased structural considerations entirely. The other was John Dalton's atomism, which held that there was only one level of structure that mattered. These conceptual idealizations were sufficiently compelling to divert the corpuscularian framework for 2 centuries.

A Materials Science Timeline

1556
Georgius Agricola's *De re metallica*, a compendium of 16th century mining, metallurgical, and general materials production, is published.

1664
Cartesian corpuscular philosophy recognizes material properties as emerging from a multilevel structure.

1665
Robert Hooke publishes *Micrographia*, which reveals levels of material microstructure never before seen.

1722
René de Réaumur publishes the first technical treatise on iron.

1782
Josiah Wedgwood develops an early form of process control with his invention of the pyrometer for measuring furnace temperatures.

1808
John Dalton publishes his *New System of Chemical Philosophy*, which establishes atomic theory.

1824
Joseph Aspdin invents portland cement, which remains one of the most used materials in the world.

1839
Charles Goodyear accidentally discovers vulcanization, which ultimately renders raw rubber latex into a widely useful material.

1856
Henry Bessemer patents a process for large-scale steel production.

We have had the past century to reinvent materials science. The atom and the continuum remain dominant philosophical forces; they are the foundation of existing theoretical tools. But armed with the growing reservoir of structural facts gleaned from instrumentation and computation, the challenge now is to adapt these theoretical tools to understand and control the complex structures of real materials.

The modern view of material structure differs from Réaumur's mainly in the detailed morphologies characteristic at the different length scales of a material's hierarchical structure. In the case of steel, the most significant difference is the overestimation of porosity in the 18th century depictions. And if Réaumur's voids are reinterpreted as "free volume," his sketch becomes a reasonable model of polymeric materials. It shows the remarkable ability of the human mind to infer necessary structure from the contemplation of properties alone.

Smith made another important historical observation about materials development *(2)*. Since prehistory, people have put newly discovered materials to practical use long before they understood much about them.

Cutting edge. Etched and repolished tip region of a 6th century sword.

Consider the pattern-welded sword blades made and used by Merovingian Franks and Vikings (see figure above) as early as the 6th century A.D. By hammer-welding steels of differing carbon content (a technical feature unknown to the early sword smiths), a laminate composite was fabricated by labor-intensive "hand lay-up" to produce a hybrid structure with a tough core supporting a hard cutting edge.

The actual mechanism of the quench hardening of steel, which is responsible for the hardened sword edge, was hotly debated even in the early 20th century. There were two factions: the "allotropists," who favored structural transformation, and the "carbonists," who pegged the hardening mechanism on dissolved carbon. A crucial observation was the discovery by Floris Osmond in 1893 of "martensite" in steel, the microstructural form that iron assumes during the quenching process. We now know that the combination of a martensitic transformation and the redistribution of trapped interstitial carbon (along with ambient aging during which additional microstructural evolution occurs) underlies the edge hardness of the 6th century swords.

The ancient swords embody another illustration of how art and craft has traditionally preceded science. The sword smiths' use of chemical etching to bring out aesthetic metallic patterns set the foundation for modern metallographic observation of microstructure established by Henry Sorby in the 19th century. By etching metal samples with acid, Sorby revealed internal microstructures and correlated them with the properties and performance of the materials.

Transmission electron microscopy (TEM), a modern analytical cohort of metallography that reveals finer structural levels (see figure at right), suggests that the ancient swordmakers ever were accidental nanotechnologists. TEM analysis reveals nanometer-scale patterns of carbon in the hard edge of the sword. These patterns emerged from a process called "spinodal decomposition", in which a solid solution, such as the sword's high-carbon martensitic steel, becomes unstable and its constituents reorganize *(3)*. In modern parlance, the swordmakers' products could be described as "self-assembled heterophase nanostructures."

The spatial dimension of materials is only part of what makes them tick. There is a spectrum of characteristic relaxation times associated with the various chemical and physical processes operating at the material's differing structural length scales. This adds the dimension of time.

The resulting dynamic spatiotemporal hierarchy means that any material at any time has structural features, such as grain sizes and dispersed particles, that have not yet reached equilibrium. That is why a material's structure and properties depend on how it was made and what conditions it endured in service.

Also fundamental to this dynamic view of materials is a realization that structural defects play vital roles at all length scales. Defects can make things fail in a thousand ways, but they're also often what makes materials so valuable. Perfect silicon crystal without dopant ions is not the semiconductor that has changed society. Pure iron metal without the right spicing of carbon would never have become the steel backbone of the industrial revolution. Although "defect tolerance" remains a central tenet of modern materials science and is of incalculable commercial and safety importance, "defect engineering" is ascendant in the minds of many materials researchers. That's because defects on various hierarchical levels are a principal opportunity for controlling material behavior.

Because the personality of each material depends on all of these interacting spatial and dynamic attributes, it makes sense to approach materials as complex systems. Smith advocated such a systems view of materials decades ago. As more contemporary practitioners live by that insight, they are finding pathways to important new materials that can catalyze advances in manufacturing tools, computers, communications systems, and the myriad technologies whose very existence or improvement depends on more capable materials.

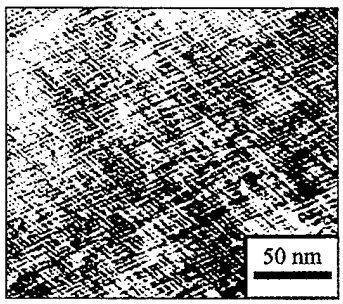

Inside steel. TEM reveals nanoscale structure of a quench-hardened steel.

The Materials Discipline Comes of Age

Two principal branches of natural philosophy have evolved to form modern materials science. One is reductionist analysis, which takes nature apart to discern and understand its fundamental units. Reductionism has operated throughout the development of science. More sporadic has been the evolution of the synthetic systems view, which is better suited for understanding the connections holding nature together. In a new balance of these two philosophies, the systems view integrates the fruits of our investment in reductionism while replacing conventional discovery-based R&D with a far more effective and efficient design-based approach.

CREDITS: (TOP) *DE RE METALLICA* (MIDDLE AND BOTTOM) G. B. OLSON

Materials by Design

To design a material is to try to meet a material user's need. A good place to start is with property cross-plots, like those of Michael Ashby, that graphically define property-performance relations *(12)*. These help engineers select materials for their product designs. They're useful for defining a quantitative set of property objectives that will sum into the materials performance needed by users. These performance specifications are determined by the role of the potential material in the wider system it serves. They also help define economic parameters, such as the cost of raw materials and processing, for the overall material design task.

With objectives and economic constraints defined, the linear three-link framework of materials science and engineering (see figure, p. 996) serves to guide the design and development phases. The Steel Research Group (SRG) (see main text) uses flow-block diagrams that represent 1) key microstructural subsystems (such as crystal grain sizes), 2) the primary links of these subsystems to the properties they control (such as strength and toughness), and 3) the stages of processing (such as tempering or reheating) that govern their dynamic evolution.

With these in hand, systems analysis is then applied to identify and prioritize key structure-property and processing-structure relations. Often, part of this exercise involves some additional modeling or empirical data gathering to fill gaps in the knowledge required for making practical decisions about composition and processing details. The systems view operates here at the strategic level, but it is supported by traditional reductionist analysis at a tactical level. On balance, the procedure greatly reduces the amount of costly experimentation in materials creation. Instead of making tens of prototypes along the way to a useful new material, SRG designers reach their target metal using only a few actual melts to refine the computation-heavy design efforts.

–G.B.O.

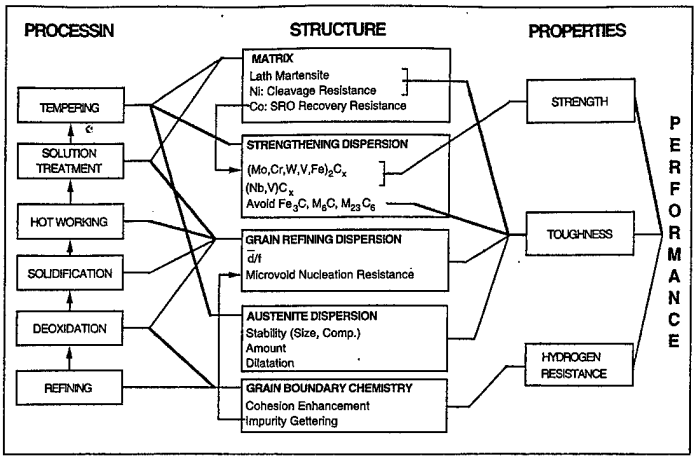

Planning materials. Flow-block diagrams guide materials design.

Although there were seeds of this turning point in materials science in early industrial laboratories at General Electric, Bell Labs, and elsewhere, the multifaceted field of materials research was deliberately synthesized as a single academic discipline in the late 1950s and 1960s with the founding of the first university materials departments *(4)*. Specialists in the science and technology of metals, ceramics, polymers, and composites collaborated in pursuit of unifying principles for the creation of materials of all classes. This meeting of minds helped lay the sociological and cognitive groundwork for a systems approach to materials.

The development of operations research in World War II and large-scale national missions such as the Manhattan Project and the Apollo space program were also important. It is estimated that at least 70% of our unprecedented economic boom of the past decade derives from technology, which in turn derives in good part from radically improved productivity via new systems-based methods of product development.

After World War II, newly formed government agencies, including the Office of Naval Research, the Defense Advanced Research Projects Agency, the National Science Foundation (NSF), and others also helped midwife the multidisciplinary sensibility needed for developing complex materials. The same was true in academe. Starting with Smith's Institute for the Study of Metals at the University of Chicago, a series of university materials research laboratories established a national infrastructure for the interdisciplinary enhancement of materials science. The private sector added sociological foundations for the emerging discipline through a diverse mix of professional materials societies, as well as the establishment of numerous materials-centered journals and conferences.

The field now consists of many thousands of practitioners who share a growing sense of community, yet whose collective expertise runs a stunning gamut of materials categories. There are synthetic diamond makers, metal alloy designers, polymer scientists, optical fiber experts, thin film ceramic makers, developers of compound semiconductors, and "biomimetic" materials researchers who aim to emulate or adapt biology's unmatched brilliance in materials innovation. The list goes on and on, with a diversity akin to the living kingdom's millions of species.

Over the past 4 decades in materials R&D, however, there has been a consistent emphasis on "good science," as defined by reductionism, rather than "good materials," which emerge when engineering, manufacturing, and economic factors are included in the mix. This bias has limited the technological impact of the materials science community, particularly the academic portion. And materials engineering per se has been left primarily to industry, which has yet to fully benefit from the expanded base of materials science.

There is a twist in store. The science of materials has reached a level at which it now can radically change engineering practice. The possibilities are akin to what has come from the relationship between the life sciences and medicine. Until the 19th century, there was little or no science to guide medical technology and practice. Since then, however, the ever growing corpus of biomedical knowledge has been leading to an ever more amazing stream of health care innovations. Here, a genuine desire to meet societal needs has produced a healthy mix of reductionist and systems viewpoints, yielding a culture that naturally integrates scientific understanding into practical use. The materials research community is poised to emulate this model.

1860s
Henry Sorby applies light microscopy to the study of the microstructure of metals and rocks.

1869
John Hyatt successfully commercializes celluloid, an artificial plastic material.

1869 and 1870
Dmitri Mendeleev and Julius Lothar Meyer publish versions of what will become known as the Periodic Table of the Chemical Elements.

1886
Charles Hall and Paul Héroult independently discover cost-effective methods for producing aluminum metal from ore.

1893
Floris Osmond discovers martensitic transformation.

1900
Max Planck formulates the idea of quanta, thereby setting the stage for the development of quantum mechanics.

1906
Alfred Wilm discovers age hardening in aluminum alloy, which is later used for making dirigibles and other aircraft.

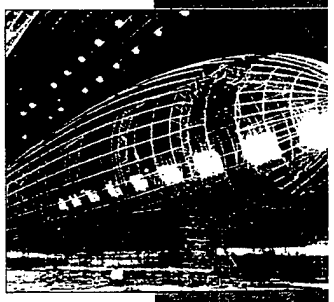

1909
Leo Baekeland patents Bakelite, the first entirely synthetic plastic, and commercializes it widely.

CREDITS: (TOP TO BOTTOM) G. B. OLSON; CORBIS

1911
Heike Kamerlingh Onnes discovers superconductivity in mercury chilled to temperatures near absolute zero.

1911–12
The father-son team of William Henry and William Lawrence Bragg, along with Max von Laue, develops the basis of x-ray crystallography, one of the most important analytic techniques for studying material structure.

1921
A. A. Griffith postulates role of defects in fracture strength.

Late 1920s
Hermann Staudinger argues that polymers are made of small molecules that link to form chains.

1934
Wallace Hume Carothers invents nylon.

1940s
The wartime practice of organizing multidisciplinary research collaborations to achieve technological goals becomes a model for the subsequent organization of a field that later becomes known as materials science and engineering.

1947
John Bardeen, William Shockley, and Walter Brattain invent the transistor.

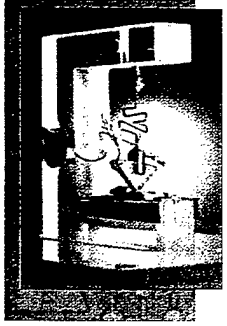

Materials by Design: Efficient Innovation

There is a general engineering design movement under way. It draws on the vast information pool generated by reductionist analysis, but adds the component of design, for which the systems approach is crucial.

Central to the materials design approach is a powerful logical structure connecting the "four elements" of materials science: processing, structure, properties, and technological performance (see figure below). By connecting adjacent pairs of these elements, a three-link chain representing a versatile materials paradigm emerges. The deductive, cause-effect logic of reductionist science flows from processing to performance. All along the way, science reveals the relevant structures and phenomena, often in astounding clarity and detail. The inductive logic of systems engineering flows the other way, from performance to processing, thereby enabling designers to arrive at specific procedures likely to yield materials with the desired sets of properties and performance.

Not often successful in terms of producing useful new materials, early efforts at materials design nonetheless were harbingers of what materials development is to become. Generally, what has made or broken past efforts was whether they included the element of design. One notable success is the work of H.K.D.H. Bhadeshia and co-workers at Cambridge University, whose ambitious assault on the complex problem of weld metal design has spawned productive efforts at several national laboratories in the United States and Japan.

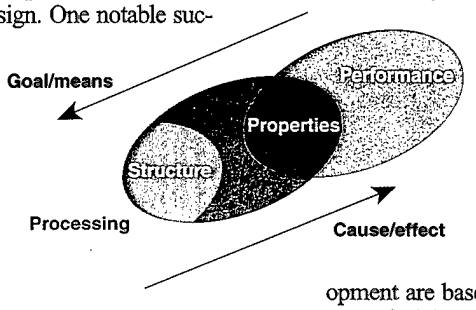

Big four. Four-element paradigm of modern materials science and engineering.

The initiative I know best is the Steel Research Group (SRG) at Northwestern University, which my colleagues and I have continuously developed since 1985 *(5, 6)*. This university-industry-government program was organized within the context of systems engineering to explore general methods, tools, and databases for the design of materials, using high-performance steels as a test case (see sidebar on p. 995). There is a faith underlying this framework: The scientific knowledge base is now robust enough to supplant the traditional, empirically driven development of materials with a more efficient theory-driven and computationally based approach (see sidebar on p. 997).

In the SRG, we begin by combining the perspectives of materials users, suppliers, modelers, and designers into a set of specific materials property objectives. Those specifications, in turn, help us define how to use, adapt, or expand science-based models and databases of material behavior. We then use these models and databases to zero in on compositions and processing protocols that can transform those compositions into alloys fitting our specifications. In the past decade, we have used this framework to develop new alloys with unprecedented sets of properties. Some are now under evaluation by industrial and government partners for use in airplanes, power generators, aircraft carriers, and other applications.

Our own projects for designing steel are just a beginning. A recent NSF-sponsored workshop on Materials Design Science and Engineering *(7)* has called for broadening this approach to the design of all classes of materials. And in recognizing materials as one of five critical technologies for U.S. competitiveness, the President's Office of Science and Technology Policy *(8)* has identified computational materials design as a principal opportunity.

Opportunities abound for application of the new systems-driven computational design approach. Successful examples from our efforts include a stainless steel bearing for a space shuttle application, high-strength, high-toughness steels for aircraft landing gear and armor applications, and a new class of ultrahard steels for advanced gear and bearing applications. The more general validity of the design approach has been explored with computational design projects focusing on nonferrous alloys, hydrate ceramics, case hardening polymers, and nanostructured thin film materials for microelectromechanical devices and hard coatings.

The new design capabilities will also help realize the dream of biomimetic materials, which emulate the complex adaptive microstructures of the living world that are beyond the reach of traditional empirical development. One successful demonstration is self-healing metallic composites. These incorporate "shape memory" alloys that exploit martensitic structural transformations to change their shape controllably. Integrating such components into thin film electronic devices to create efficient microactuators is leading to smart materials systems that unite the worlds of structural and electronic materials. Here the growing philosophy of predictive materials design is now combining the electrical engineer's realm of perfection-driven, artificially structured microcircuits with the materials traditions of self-assembly *(9)* and defect tolerance *(10)*.

Following the same philosophy can reduce the cost of discovery. In contrast to computational materials design, the prevalent industrial methods of materials development are based on an intrinsically slow and expensive process of trial-and-error empiricism. Theoretical input has been qualitative at best. It typically takes tens of millions of dollars over 2 decades to fully develop and qualify a new material in a critical application *(11)*. This sluggishness stands out in an era when engineers are expected to deliver new generations of products, such as automobiles, on an 18-month cycle. What's more, under these competitive pressures many industrial materials-development groups have been severely reduced or closed over the past decade. A recent National Research Council study *(11)* has concluded that the greatest challenge to the materials field today is the short time and cost constraints of the full materials development cycle.

Another reason these industrial materials development efforts have been downsized is anchored in the old R&D model in which new materials are discovered rather than designed. A typical estimate is that $1 of discovery costs $10 of development. If eliminating that first dollar was the only advantage of computational materials design, its impact on the total discovery and development cost would be small. The real advantage of materials design is that good design in the first place requires much less development later. And rather than using materials design approaches simply to provide an initial prototype for subsequent empirical development, there's yet more to be gained by integrating predictive modeling throughout the full design and development process.

Consider two costly and time-consuming phases of the standard materials development cycle: process optimization and qualification testing. A major concern in process optimization is scale-up. Because processing phenomena such as heat transfer depend on product size, a prototype material investigated on a small scale is not likely to behave the same way when processed on a large scale. "Solidification design" can preempt

CREDITS: (TOP TO BOTTOM) G. B. OLSON; LUCENT TECHNOLOGIES' BELL LABS

Virtualizing Materials to Create Real Ones

Design of the hierarchical structure in materials requires a hierarchy of models based on materials science, applied mechanics, and even quantum physics (see figure at right). Models to help design features on the coarsest structural level of solidification, such as the chemical banding visible in the patterned sword blades mentioned earlier, employ powerful thermodynamic codes such as THERMOCALC *(13)*. These models enable designers to simulate the 10-μm scale of structure. In metal alloys, this is the level at which the chemical partitioning between liquid and solid phases evolves during solidification processing. Application of these models aids decision-making about thermal processing details, a practice we like to call "solidification design."

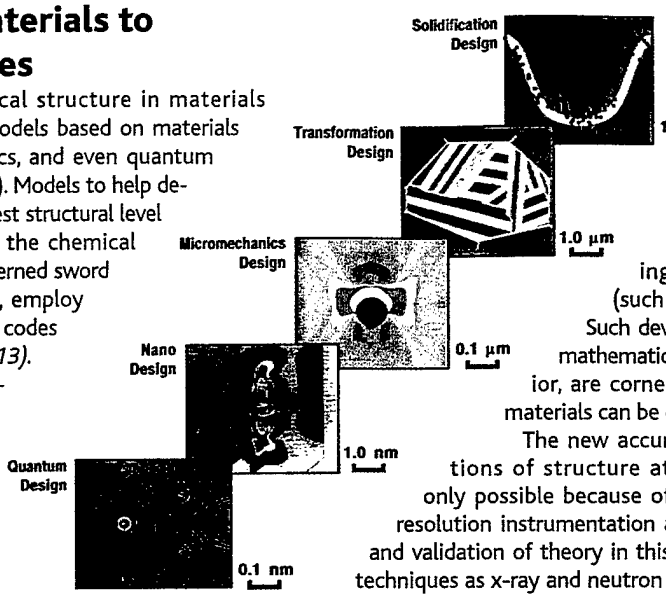

Model relay. Computational design of materials requires a hierarchy of models.

At the 1.0-μm scale of structure, "transformation design" is the goal. This concerns the evolution of structural changes during quenching, whereby crystal grains present at high temperatures transform and subdivide as the hot alloy cools into a hierarchy of lower temperature crystalline units. The design goal here is to specify and control processing temperatures so that desirable microstructures will form, while hindering the formation of competing microstructures that are less beneficial.

The 0.1-μm scale represents the micromechanics design level. An example of the phenomena relevant at this scale is "grain refining," in which the large grains formed at high temperatures that can embrittle alloys are made smaller by more precise thermal or compositional control. There's a trade-off here, because more smaller particles can also catalyze ductile fracture (breaking, that is), as there are more interfaces that can separate from one another. Micromechanics models typically are based on continuum descriptions of mechanical phenomena that can simulate the evolution of microstructures during material deformation and fracture.

In recent years, an even finer structural level—the nanoscopic level—has become better understood and more controllable. The control of 1-nm-scale particle dispersions in alloys created through solid state precipitation during "tempering" at intermediate temperatures, for example, provides efficient obstacles for resisting plastic deformation. Said differently, this nanometer-scale structuring strengthens the metal.

The development of design models for these diminutive scales builds on a half-century evolution of theory for both precipitation and strengthening in metals. A major materials science breakthrough of the 1950s was the identification of dislocations as the key defects that enable the sliding of crystal planes, which shows up as plastic deformation of many materials. While most structure-property relations, such as the Hall-Petch relation for grain refinement strengthening, are based on empirical correlations, a major triumph of the 1960s was the Orowan particle strengthening equation. Derived directly from dislocation theory, it relates strength to the inverse spacing of dislocation obstacles (such as nanoscale precipitates). Such developments in theory, which mathematically codify materials behavior, are cornerstones for the claim that materials can be designed largely in silico.

The new accuracy of theoretical predictions of structure at the nanometer scale is only possible because of recent advances in high-resolution instrumentation allowing precise calibration and validation of theory in this regime. This includes such techniques as x-ray and neutron diffraction, various electron microscopies, and atom-probe microanalysis. The latter is represented by the three-dimensional atomic reconstruction of a 3-nm strengthening carbide particle in an ultrahigh-strength steel shown below. Such new capabilities in structural and chemical analysis down to the atomic scale open a new era of quantitative materials nanotechnology.

The electronic level is the finest level relevant to real materials. This is the realm of quantum design. As acknowledged by the 1998 Nobel Prize in chemistry shared by John Pople and Walter Kohn, the development of computational quantum mechanics and its extension via density functional theory constitute a profound advance that already has had significant industrial impact. A collaboration of materials science, applied mechanics, and quantum physics has enabled some of us in the Steel Research Group (see main text) to apply computational quantum mechanics to engineer steel at the subatomic level.

Our approach was to recast models of the impurity-induced embrittlement of grain boundaries into thermodynamic terms *(14)* and to rely on precise models of the atomic structures at grain boundaries. As represented by the computed valence charge density contours for a phosphorus atom at the core of an iron grain boundary, total energy calculations are sufficiently precise and accurate to explain the known effects of interstitial components such as boron, carbon, phosphorus, sulfur, and hydrogen on the cohesion of iron grain boundaries. What's more, the calculations lead to new mechanistic insights at the electronic bonding level. Extension to elements that occupy substitutional Fe sites in the boundary has enabled us to predict new alloying elements for enhancing boundary cohesion in steels. This is creating a new generation of "quantum steels" that incorporate these properties derived directly from electronic-level predictions. **–G.B.O.**

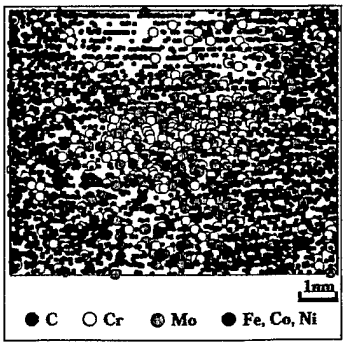

Atomscapes. A view of a Cr-Mo carbide particle that strengthens steel alloy.

CREDITS: G. B. OLSON

1950s to 1960s
Much of the theoretical foundation behind the formation and evolution of material microstructure is developed. Among them is the Hall-Petch relation for grain refinement strengthening and the theory of diffusion of solids.

1953
Karl Ziegler develops catalysts that make it easier and cheaper to polymerize ethylene into stronger, more capable polymers.

1955
A team of scientists at General Electric combine high temperatures and enormous pressures to create synthetic diamond.

1957
John Bardeen, Leon Cooper, and John Schrieffer provide theoretical basis for superconductivity, discovered in 1911.

1959
The U.S. government funds the first IDLs, or interdisciplinary laboratories, which mark a beginning of the modern academic model of materials science and engineering.

J. W. Cahn and J. F. Hilliard develop theory of microstructural evolution in diffuse-interface systems.

1970
Researchers at Corning develop optical fibers transparent enough to make fiber optic communication practical.

1974
A study by an NAS committee, COSMAT, defines field of materials science and engineering, creating a community sensibility.

1980
Gerd Binnig (right) and Heinrich Rohrer (left) invent scanning tunneling microscopy, which has led to a family of imaging tools often capable of molecular- and atomic-scale resolution.

1985
First university "materials by design" initiatives attempt computational materials design.

1986
K. Alex Müller and J. Georg Bednorz discover high-temperature superconductivity in ceramic materials.

1990s
The field of materials science and engineering begins shifting into a more systems-based approach to materials innovation and toward materials design in which researchers can predict new materials they would like to have rather than having to discover them.

this common showstopper. By using models that simulate how materials respond to processing conditions for designing a material at the ultimate process scale of interest, we can reduce the number of expensive large-scale experiments while shortening the development cycle.

Improving qualification testing is more challenging. To design with confidence, designers must know how properties vary within the materials they intend to use. Current practice requires much testing to define these variations statistically. But most structure-property theories provide mean values of the variables of interest; they do not tell a designer about location-to-location variations within materials.

Help is coming, however. Researchers are developing a probabilistic materials science whereby structural distributions are mapped into property distributions. These are the kinds of data designers can use to make better predictions about how different materials will affect their products. Models of this kind already exist for fracture properties and heterogeneous phase transformations, and more efforts are being planned for this vitally important area.

Each month, Britannica.com enhances the Pathways of Discovery essay with links to relevant items within and without *Encyclopedia Britannica*'s vast stores of information. To access this month's Pathways essay and all previous ones, go to www.britannica.com and click on the "Science" channel.

Structure of Education

Education offers the most leverage for moving materials R&D into the systems-based paradigm. In its post-Cartesian form, modern metallurgy began with an emphasis on the direct correlation of processing and properties. The advent of physical metallurgy a century ago opened the "black box" of structure and brought a revolution in the fundamental understanding of the mechanistic link between processing and properties. This understanding created the foundation for the more recent generalization to materials science, making possible the general materials design and systems engineering methodologies described in this essay. Given the demonstrated potential of materials design, institutionalizing it via education would result in many benefits to society.

Due to the historic dominance of reductionist philosophy, however, we now have in place an analysis-oriented education system. In the name of objectivity, we train students to shut down the more synthetic and emotional tools of thought, which are precisely the ones best suited for doing good systems engineering. The future of engineering education, therefore, ought to target these subjective reasoning powers.

An activity of our new materials engineering curriculum at Northwestern, the Dragonslayer Project, is designed to do this. The project explores the design of an "aesthetic" material through collaboration of freshman and upperclass design teams. The widespread presence of Western dragon combat in literature is used to integrate frontier steel technology with the history and legend of swordmaking to design an ultrahigh-performance sword that our market analysis shows would be of maximum value to sword collectors.

Much of the mystique of the legendary Samurai sword, which even 5 centuries ago achieved performance levels equivalent to those of a modern carburized blade, stemmed from its ability to cut through other swords of the day. The equivalent performance advance has been adopted as a benchmark for property requirements.

Fanciful as the project might seem, it's no different from the kind of materials design that goes on at the DuPonts and Cornings of the world. Searches of literature, albeit medieval literature, were used to determine technical specifications, including the need for flame resistance when fighting fire-breathing dragons. Historians of the Dark Ages helped to identify and select a historically accurate sword style—the patterned double-edge broadsword. And market analysis helped determine what the target buyers, sword collectors, would be willing to buy and how much they might pay.

Finite-element mechanics simulations of cutting through a modern carburized blade led to a conceptual design for radical surface-hardening technologies to achieve this ambitious sword-cutting objective. We also were guided by the unlikelihood that anyone would face supernatural evil armed only with technology. This led to an additional design parameter, which market surveys indicated would constitute an important attribute in a collectible dragonslaying sword: The sword should be made from material of heavenly origin, namely, meteoritic iron. This is a technical feature with historical and legendary precedent (including the Excalibur legend).

Our systems approach to materials design has established the feasibility of using tabletop-scale aqueous electrolytic refinement of available meteoritic iron to achieve the necessary purity for producing the unprecedented alloy steel performance needed for a sword fit to defeat the most evil of adversaries. The freshman design team's proposed market plan includes auctioning a single "techno-mystical" sword for publicity, followed by commercial marketing of a range of high-performance steel products, including the "Dragonslayer golf club."

In this millennium, a new architecture of synthetic thought will continue its symbiosis with modern computational capabilities. And an age of empirical exploration will continue to be superceded by an Age of Design. This will open up powerful pathways by which human creativity, fused with scientific knowledge, will bring new levels of control over the material world widely applicable both to society's problems and its ambitions. The manifestation of the design paradigm, whether in an undergraduate or corporate setting, corresponds to a form of transmutation beyond the alchemist's dreams: the creation of materials from thought.

References

1. C. S. Smith, *A Search for Structure* (MIT Press, Cambridge, MA, 1981).
2. C. S. Smith, *A History of Metallography* (MIT Press, Cambridge, MA, 1988).
3. K. A. Taylor *et al.*, *Metall. Trans.* **20A**, 2717 (1989).
4. I. Amato, *Stuff: The Materials the World Is Made Of* (Basic Books, New York, 1997).
5. G. B. Olson, M. Azrin, E. S. Wright, Eds., *Innovations in Ultrahigh Strength Steel Technology*, Proceedings of the 34th Sagamore Army Materials Research Conference, 1990.
6. G. B. Olson, *Science* **277**, 1237 (1997).
7. D. L. McDowell and T. L. Story, "New Directions in Materials Design Science and Engineering," National Science Foundation Workshop Report, Georgia Institute of Technology Materials Council, Atlanta, GA, 1999.
8. "New Forces at Work: Industry Views Critical Technologies," 4th Office of Science and Technology Policy Report on Critical Technologies, February 2000.
9. G. M. Whitesides, J. P. Mathias, C. T. Seto, *Science* **254**, 1312 (1991).
10. S. Williams, *Technol. Rev.* **102**, 92 (September/October 1999).
11. D. Stein, *MSE: Forging Stronger Links to Users* (National Research Council, Washington, DC, 1999).
12. M. F. Ashby, *Materials Selection in Mechanical Design* (Pergamon, Tarrytown, NY, 1992).
13. L. Kaufman and H. Bernstein, *Computer Calculation of Phase Diagrams* (Academic Press, New York, 1970).
14. J. R. Rice and J.-S. Wang, *Mater. Sci. Eng.* **A107**, 23 (1989).

Gregory B. Olson is Wilson-Cook Professor of Engineering Design in the department of materials science and engineering and director of the Materials Technology Laboratory at Northwestern University.

Matrix Alloys for Kinetic Energy Antitank Applications

Andrew Elliott
Professor Olson

Abstract-

In recent years the US military has come under increasing criticism regarding its environmental record. One area of contention has been the use of depleted uranium in its weapons and armors. As an antitank penetrator uranium-titanium (U- .075 wt. pct. Ti) has shown to be more effective that current tungsten (W) substitutes due to the density of the alloy and the effects of shear localization at the point of penetration. It is the shear localization, which reduces the amount mushrooming in the head of the weapon, increasing the penetration depth.

Despite several in-depth research studies no suitable material replacements have been found with this performance characteristic. However with current techniques, it is possible to design materials that not only undergo shear localization but that do so at the same point as the U-Ti alloy.

Experiments were performed on Hf-Ta alloys to observe a martensitic to austenitic phase change. The atomic weight percent of the alloy was roughly calculated to get a T_0 temperature for the martensitic to austenitic, α (HCP) to β (BCC), phase change, at 700°C using a straight-line method. Results from the experiments provide evidence that a martensitic phase structure is achievable using these calculations. The presence of this phase indicates that the subsequent transformation to austenite should be possible and that the system should provide the necessary shear localization properties required in a U-Ti replacement alloy.

Further refinement of the T_0 temperature calculation was performed with the use of ThermoCalc, a computer modeling program, providing a more accurate representation of the T_0 temperature for the α (HCP) to β (BCC) phase change. Future research and experimental results will allow this model to become more accurate, to the point where a substitute alloy can be designed for the U-Ti system without any degradation in performance.

June 2000

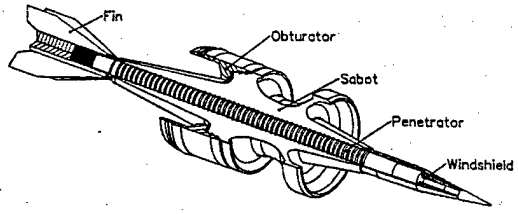

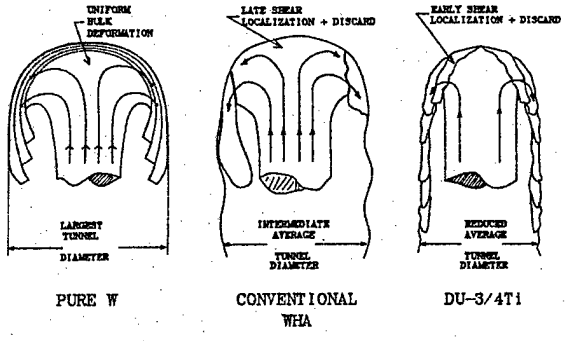

Figure 1: A cut a way view of a typical penetrator. Figure 2: The result of impact on W and U alloys (ARL)

Introduction-

While the end of the Cold War has reduced the threat of war, the battle on the materials science frontier rages on. The change in roll of the military as it becomes a policeman and peacekeeper, means that it must also change its approach to fighting. No longer is it acceptable to win at all costs. Increasing concern for the lives of its soldiers, civilians and the environment dictates the way in which the US military performs its current roles.

Due to environmental concerns, the military has been trying to develop a tungsten (W) replacement for the depleted uranium-titanium (U-0.75 wt pct Ti) alloy that it currently uses in its kinetic anti-tank penetrators (Figure 1). Tungsten alloys, however, have shown to be considerably less effective in these applications, due to the plastic deformation that occurs when tungsten penetrators hit a target. The ability to design and model material systems, means that it is possible to replicate the properties of the U-Ti alloy in a tungsten system.

The overall goal of the project is to be able to give a tungsten alloy the shearing

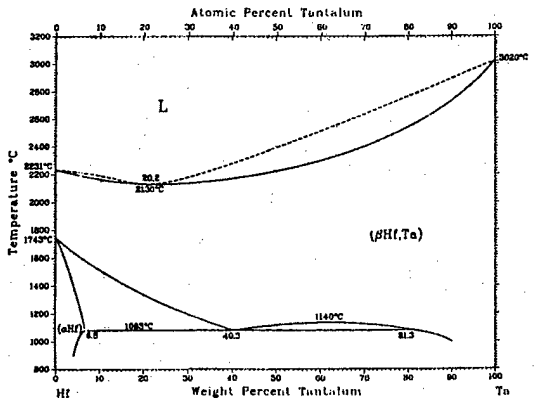

Figure 3: The Hf-Ta phase diagram [2]

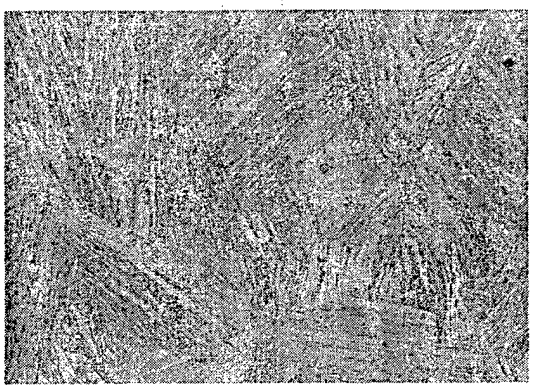

Image 1: A martensitic phase in low carbon steel

properties that will allow it to have similar or better performance characteristics than the existing U-Ti system.

The approach is to design an alloy that exhibits shear localization (Figure 2) and that when used as a matrix alloy with tungsten will provide a system that exhibits overall shear localization.

The matrix alloy is expected to compose around 30% of the tungsten penetrator.

With this in mind the system that was chosen as the matrix alloy for these experiments was hafnium-tantalum (Hf-Ta) (Figure 3). The most important aspect of this system is the diffusionless phase change (α-β), which is expected to provide the shearing mechanism. Additional consideration was also given to the fact that these alloys share similar densities and processing characteristics with tungsten.

The structure of the project is well outlined by Northwestern's Materials Science department's approach of looking at the relationship between Performance-Properties-

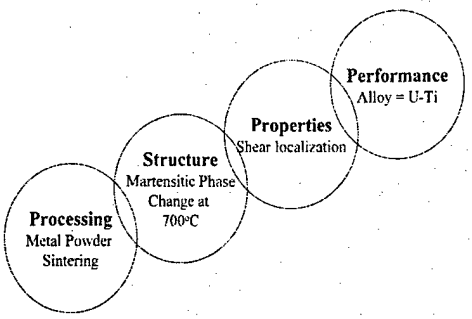

Figure 4: Project goals

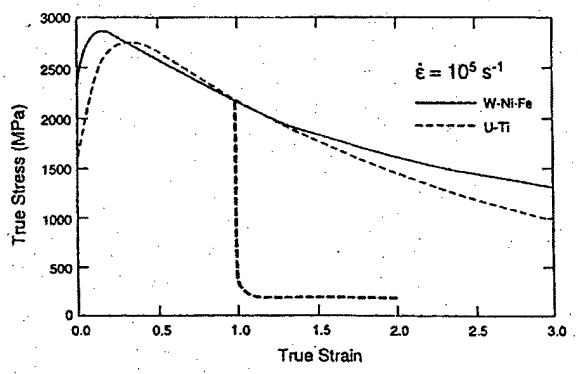

Figure 5: The stress vs. strain curve for U-Ti [3]

Structure and Processing (Figure 4). The overall goal of the project was determined by the performance requirements set by the current U-Ti alloy.

The major property of the U-Ti alloy system that is directly responsible for the current alloy's overwhelming performance advantage is shear localization (Figure 5). This figure shows the stress verse strain curve for the actual U-Ti alloy, a typical W alloy, and a computer model of expected U-Ti curve. The dramatic drop in the actual stress as the stain increases means that excess metal shears off instead of plastic deforming and inhibiting further penetration.[4]

The structure, which facilitates the shearing process, is a diffusionless phase transformation, in the case U-Ti β-γ. In the Hf-Ta alloy system the phase change from α-β (BCC to HCP) is expected to result in a similar affect. This affect has been observed in steel systems where there is a martensitic to austenitic phase change. By manipulating the composition of the alloy the temperature at which phase change occurs can be selected.

The details of final subdivision, processing, were determined by Hf-Ta system. The use of these refractory metals limits the options available to make a homogeneous alloy due to their high melting temperatures. This provides two possible options for the manufacturing of samples, powder sintering and vacuum arc melting. Powder sintering was used in these experiments.

Literature Survey-

Literature showed that quite a bit of previous work had been done both to analyze the U-Ti system and to develop tungsten substitutes. However at this time not much progress has been made in creating a tungsten alloy that meets the material performance requirements. The most important of these requirements being the ability of the penetrator alloy to undergo re-sharpening via shear localization.

In order to simulate a ballistics impact the Hopkinson bar test appears to be favored due to the high compression rates that can be simulated. Testing on current U-Ti and W alloys has shown that this test produces accurate results relative to actual field performance. [5]

No current tungsten heavy alloy, WHA, has been found that shows the shear localization effect. Mechanical testing of these alloy results in mushrooming at the head of the sample (Figure 2). U-Ti samples show a sudden failure and load drop in the stress strain curve, a sign of the shear localization. This is due to the β to γ phase transformation in the U-Ti system which occurs at a range in strain of .8 to 1.0 depending on the strain rate. Through mechanical testing it has been found that the strength of the U-Ti alloy drops significantly

when deformation proceeds in the high temperature γ phase.[6] Current W alloys exhibit no such similar behavior.

Research on steel has shown a correlation between a diffusionless martensitic phase (Image 1) change and early failure due to shear localization. The shear localization process relies on shear band formation and subsequent failure through shear band interaction, & ductile rupture of the material. This causes the penetrator to efficiently eject excess material at the head of the weapon and penetrate further into armor material.

Thermodynamically T_0 temperature is the temperature at which the molar Gibbs energy of BCC and the HCP phases are equal.

$$G_m(\alpha)|_{XTa} = G_m(\beta)|_{XTa}$$

Above this temperature the diffusionless α to β transformation can take place. However partitioning by diffusion can also still occur at longer time scales.[7] Modeling the alloy from this thermodynamic information should provide the necessary phase change.

Experimental Procedure-

The samples were designed to achieve the martensitic to austenic phase change that is necessary for the shear localization. A rough approximation was made on the phase diagram using a straight-line method intersecting the point halfway between the Hf_α and eutectic. This resulted in the following equation denoting the approximate T_0 temperature for the phase change:

$$y = -2803x+1743$$

Where x is weight percent tantalum and y is the T_0 temperature in degrees Celsius. In order to achieve a T_0 of 700°C the equation required 37.21 wt. pct. Ta.

From this calculation Ta (13.9g) and Hf (29g) metal powders, –325 mesh (44μ), were mixed using a ball milling process (Process flow chart 1). This was done in a N_2 atmosphere with steel ball bearings for half an hour. The powder was then pressed using isothermal pressing at 50,000 lbs resulting in a sample that was approximately 20cm x 3mm diameter. This sample was then divided into four smaller samples (12.2g, 9.9g, 8.7g, 6.4g)

Two of these samples (12.2g, 9.9g) were then placed in a tungsten furnace and melted in an argon furnace above 2600°C. This temperature was held for about five minutes (Process flow chart 2). These conditions were caused by a faulty reading from the thermocouple and caused the Hf-Ta system to form a liquid, essentially casting it in the graphite crucible.

The formation of the alloy by this method caused some of the Ta components to separate creating an inhomogeneous mixture. This is further covered in the results and discussion section. Five samples, 10mm by 2mm in diameter, were cut from the cast piece using electrical discharge machining (EDM). These will be referred from here on out as the tungsten furnace samples.

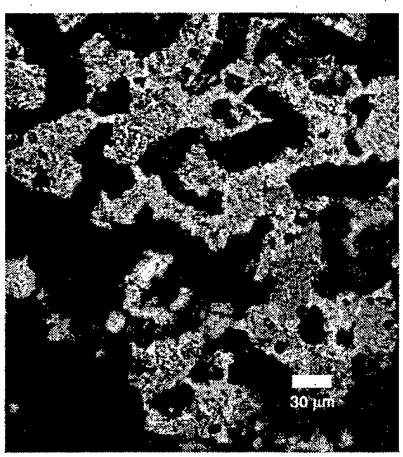

Image 2: Micrograph of sintered sample

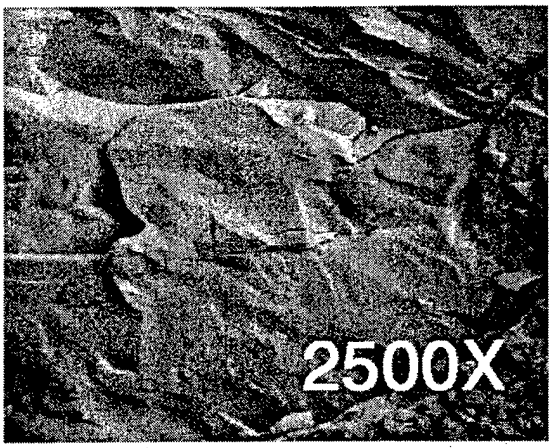

Image 3: SEM photo of pre-etched tungsten furnace sample surface

Another attempt to sinter a sample was performed at 1850°C for 1hr. in an Ar atmosphere (Process flow chart 3). The physical constraints of the furnace required that the sample be smaller than the original size. This requirement resulted in a sample that was 1.5 cm long and 3mm in diameter.

Since this sample was sintered for a relatively short time, 1hr. verse our target of 24hrs. the result of this was that the sample was not fully dense as the micrographs show (Image 2).

Surface analysis of the sintered sample also showed several large cracks running through the sample. These likely occurred due to a temperature gradient inside the furnace. The porosity of the sample also made it very brittle and along with the surface cracks made processing for further testing difficult. This sample will be referred to as the sintered sample.

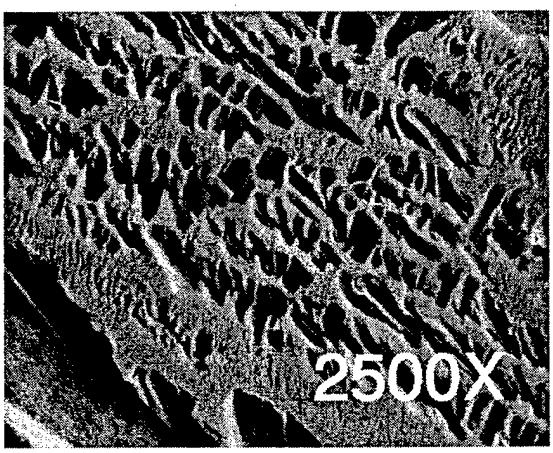

Image 4: A post-etched SEM photo of tungsten furnace sample

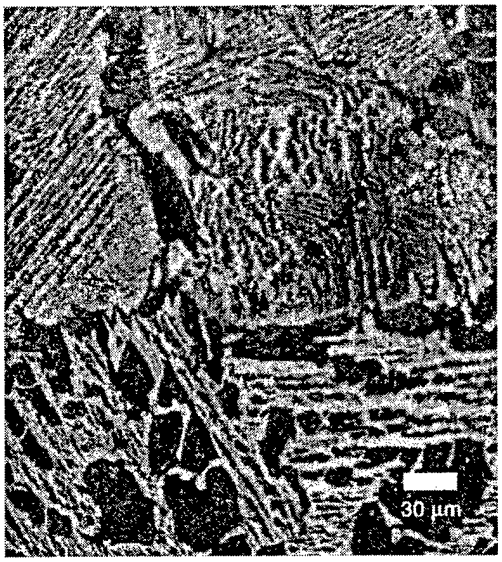

Image 5: The microstructure after solution treatment

Energy Dispersive Spectroscopy was performed on a tungsten furnace sample using the 3500 scanning electron microscope (SEM) at 20KeV both prior (Image 3) to and after (Image 4) etching. This was done to ensure that no contamination had occurred with the heat shields due to the high furnace temperatures. Counts were collected and analyzed by the Imix program (Process flow chart 4). Hf, Ta, Mo, C elemental K lines were inserted over the spectrum (Figure 5).

The tungsten furnace samples were solution treated after some initial dilatometer testing. It was hoped that this would improve the microstructure. This was done in an argon atmosphere at 1200°C for 1hr. The samples were then quenched in oil (Image 5).

One sample of each type (cast, cast-solutionized, sintered) was mounted in a cold mount and polished using 240, 320,400,600 grit sand paper followed by 30, 6,1µm water based

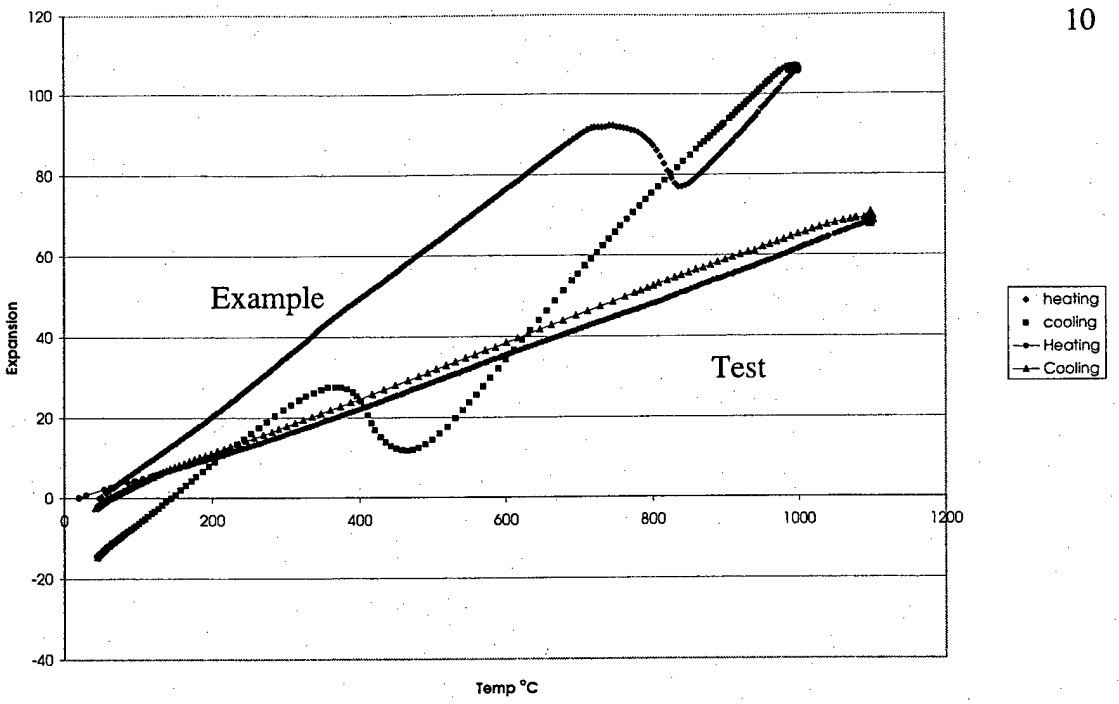

Chart 1: Typical hysteresis from a phase change and a result from the tungsten furnace samples

diamond polisher and .03μm alumina solution. Between each step the samples were cleaned with soap in an ultrasound and washed with methanol between polishing steps.

To enhance visual analysis Hf etching of the grain boundaries was performed using a HF etchant (10ml HF, 45ml HNO_3 , 45ml H_2O). The sample was swabbed for fifteen seconds to enhance the grain boundary definition. This assisted greatly in the analysis of the microstructure which became much more apparent after etching. Digital pictures were taken under 200, 400, and 1000x magnification.

Three kinds of samples measurements were taken on the dilatometer, tungsten furnace pre-solution treated samples, tungsten furnace post solution treated samples, and a sintered sample. The dilatometer measures the relative change in length vs. the change in

temperature. It is from these experiments that a T_0 temperature can be calculated from the hysteresis (Chart 1). By finding the austenitic start (A_s) temperature and martensitic start (M_s) temperature, denoted by a 1% change from linearity, the average of these two temperatures can be used to find an approximate T_0 temperature. Further statistical manipulation can be performed to increase the calculations accuracy.

A number of experiments were run in the dilatometer from 45°C to 1100°C on tungsten furnace samples, 10mm x 2mm, at the heating rate of 100°C/min. The samples were then held at 1100°C in an inert atmosphere for either 2 or 10 min., and rapidly or slowly cooled over a period of seconds (Table 1). An attempt to do a measurement of the sintered sample was made. This sample was prepared by using the low speed saw to cut a section off of the overall sample and then using the saw to ensure that the ends were parallel. However an accurate reading was not possible due to trouble attaching the thermocouple to the surface of the sample.

Vickers hardness testing was performed on all three types of samples in the cold mount. The Vickers testing was performed under a 200g load for five seconds (Table 2).

Results and Discussion-

Both tungsten samples, pre and post solution treated, were unable to produce a hysteresis in the dilatometer. Despite the fact that the samples were solution treated to create a more

Image 6: Ta dendrites

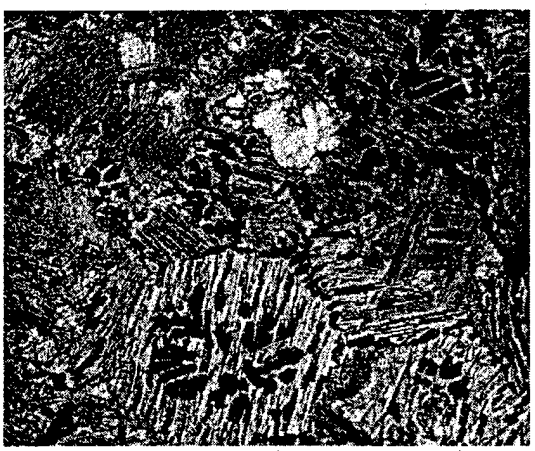

Image 7: Post Solution treated samples with suspected Ta inclusions

homogeneous ~~mixture~~ structure none of the trials showed enough deviation to determine an A_s and M_s temperature. Ten different trials were run manipulating the heating rate, holding time, and cooling rate (Table 1).

These results were due the inhomogeneous nature of the sample caused by phase separation due to the liquid to solid phase transformation, which produced Ta rich dendrites (Image 6). Also due to the short amount of time that the solution was in the liquid phase it is likely that not all the Ta powder metal melted into the liquid (Image 7). This was confirmed in the post solution treated sample which showed areas of 100% Ta during EDS analysis. Pulling Ta out of the system would have created a composition that had less wt. pct. Ta than indicated by the initial calculations making a diffusionless transformation more unlikely at 1100 °C

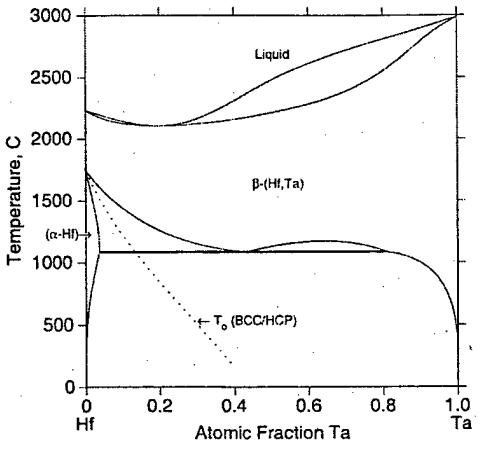

Figure 6: ThermoCalc T_0 calculation for Hf-Ta [8]

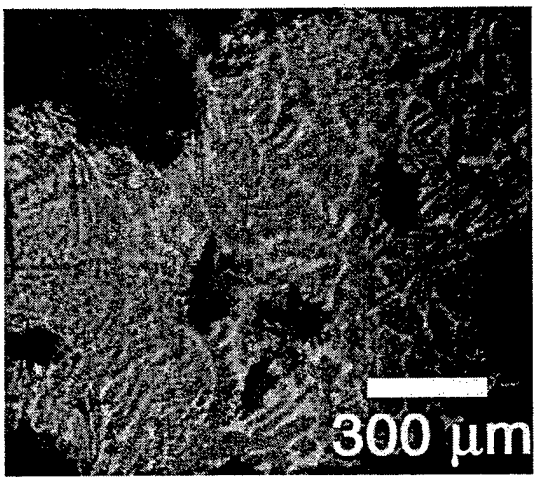

Image 8: Sintered sample showing martensitic like structures

Microstructural analysis of the post-solution treated samples shows some favorable results as far as the presence of a martensitic phase structure. When these photos are compared to that of martensitic regions in low carbon steel, the microstructure looks very similar (Image 7). This phase was not great enough to dominate the overall sample properties though since no phase change was detected in the dilatometer.

Or volume change was too small

The powdered sintered sample was very brittle and extremely porous due to the short sintering time that was dictated by the high temperature Ar furnace. Due to problems welding the thermocouple on the sintered samples no reliable dilatometer results were attainable. However microstructural analysis of the post-etched sintered sample also shows features that look martensitic (Image 8).

While hardness data was difficult to ascertain and varied dramatically over the sintered specimen do the porosity of the sample. Two microhardess tests showed a Vickers

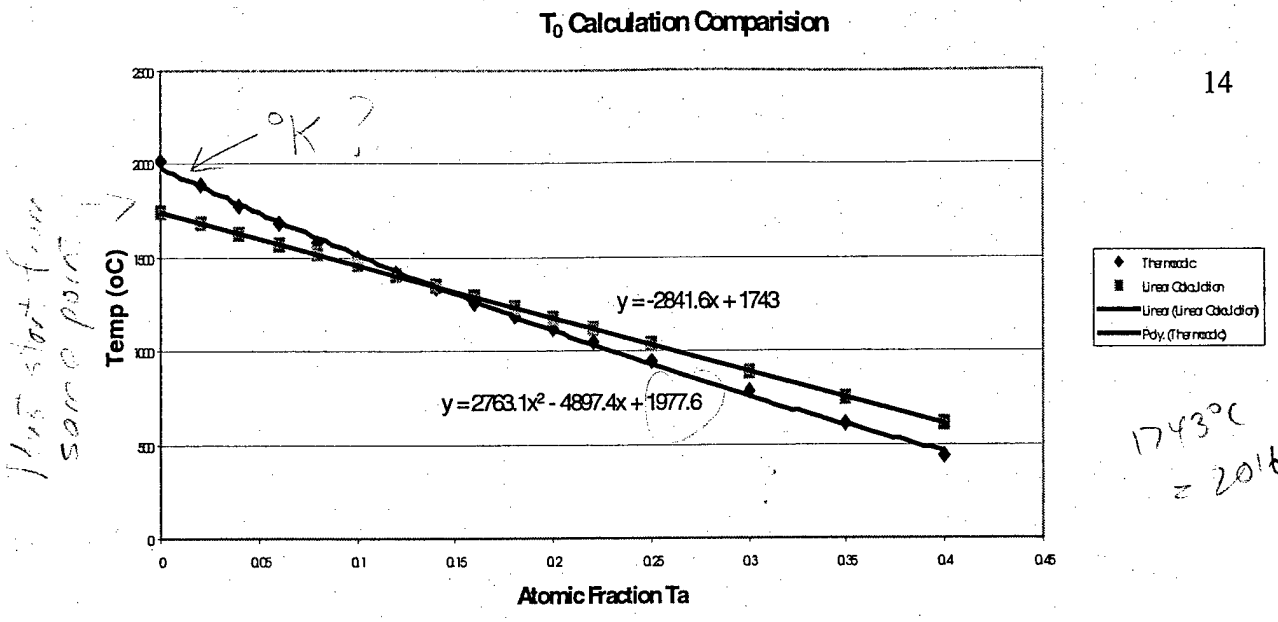

Chart 2: A comparison of the straight-line approximation for T_0 with the ThermoCalc modeling

hardness of 753 and 841 significantly higher than the fully dense samples. This dramatic rise in hardness is also likely due to a martensitic phase.

The ThermoCalc T_0 calculation from the Hf-Ta phase diagram results in the following equation (Figure 6).

$$y = 2763.1x2 - 4897.4x + 1977.6$$

Where x is the atomic fraction of tantalum and y is the T_0 temperature in degrees Celsius. As expected this differs from the rough estimate provided by the straight-line method (Chart 2). Further refinement of this equation will be possible with experimental data. However this calculation provides considerable improvement as a starting point for future experiments.

Conclusions-

The results of the testing on the Hf-Ta powder sintered sample shows that it is possible to create martensitic regions in the system. This means that although a specific T_0 temperature for the phase change was not confirmed experimentally this was a successful first step. The modeling of the T_0 temperature from the Hf-Ta phase diagram allows for a more accurate composition to be calculated. Future work with the Hf-Ta system should allow for tailoring of a tungsten alloy to the penetrator application.

Acknowledgements-

I would in to thank the following people for their assistance with this project.
Professor Olson – Advising
Professor Johnson – Metal powder sintering
Dr. Gautam Ghosh – ThermoCalc modeling
Dr. Jingha Wang – High temperature argon furnace
Dr. Kathleen Stair – Micrographs
Dr. Charlie Kuehmann – Phase diagram analysis
Rick Kramer – Dilatometer
Mathew Henrichsen – Furnace issues

List of References-

Alloy Digest, Alloy Digest, 1994. pp Hf-1, Ta-2

Massalski, T., *Binary Alloy Phase Diagrams*, ASM International pp2114-2115

Zurek, A. and Follansbee, P., *A Comparison of Shear Localization Susceptibility in U-0.75 Wt Pct Ti and W-Ni-Fe during High Strain Rate Deformation*, Metallurgical and Materials Transactions A, Vol. 26A, June 1995, pp 1483-1490

Weerasooriya, T. and Magness, L., *High Rate Testing of Kinetic Energy Penetrator Materials*, Materials Directorate, Army Research Laboratory Aberdeen Proving Ground, MD 21005, pp 1-7

Magness, L., *Ballistic and Instrumental Mechanical Testing of Long Rod Kinetic Energy Penetrator Materials*, Proc 3rd International Conference on Tungsten and Refractory Metals, McLean VA, 1995, pp133-144

Porter, D. and Easterling, K., Phase Transformations in Metal and Alloys, Chapman and Hall, 1992, pp 1-47, 382-416

Goldstein, J., Scanning Electron Microscopy and X-Ray Microanalysis, Plenum, 1994, pp 64-68, 343-356

Shackelford, J., Introduction to Materials Science for Engineers, Prentice Hall, 1992, pp167-188

Gaskell, D., Introduction to the Thermodynamics of Materials, Taylor and Francis, 1995, pp 170, 442-446

Citations-

1 Magness, L., *Ballistic and Instrumental Mechanical Testing of Long Rod Kinetic Energy Penetrator Materials*, Proc 3rd International Conference on Tungsten and Refractory Metals, McLean VA, 1995, p 134

2 Massalski, T., *Binary Alloy Phase Diagrams*, p 2115

3 Zurek, A. and Follansbee, P., *A Comparison of Shear Localization Susceptibility in U-0.75 Wt Pct Ti and W-Ni-Fe during High Strain Rate Deformation*, Metallurgical and Materials Transactions A, Vol. 26A, June 1995, p 1489

4 Ibid, 1484

5 Weerasooriya, T. and Magness, L., *High Rate Testing of Kinetic Energy Penetrator Materials*, Materials Directorate, Army Research Laboratory Aberdeen Proving Ground, MD 21005, pp 1

6 Zurek et al, 1489

7 Gaskell, D., Introduction to the Thermodynamics of Materials, Taylor and Francis, 1995, p170

8 Calculations performed by Dr. Gautam Ghosh, 2000

9 Joseph Goldstein, Scanning Electron Microscopy and X-Ray Microanalysis, Plenum, 1994, pp 343

SEM (EDS) Analysis

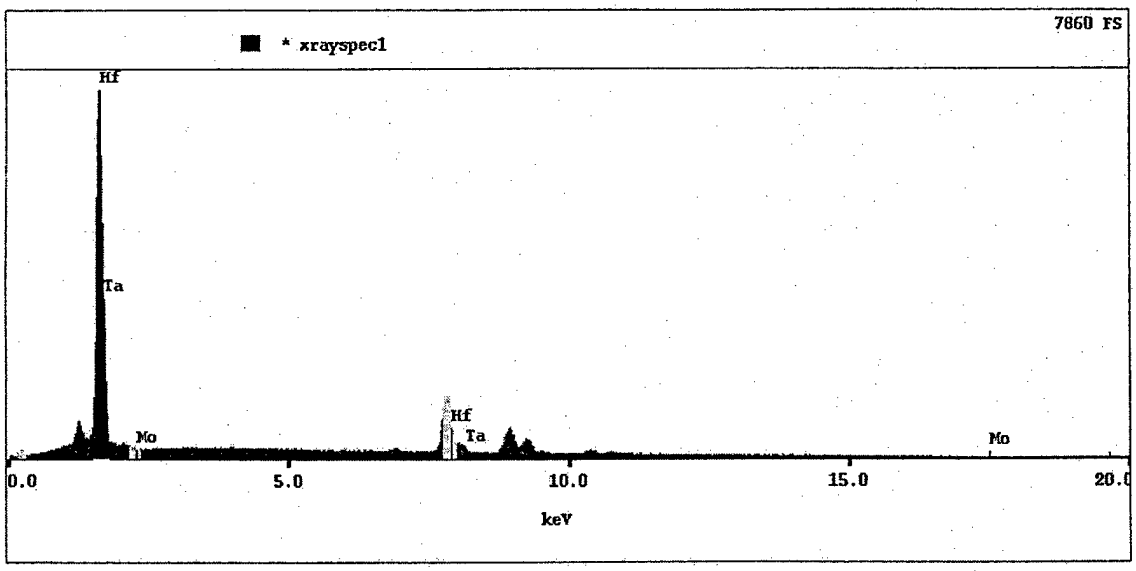

Pre-solution treatment EDS readings

Element	Point 1	Point 2	Point 3	Point 4	Average wt%	Var	stdev
Ta	0.00	0.42	0.64	0.62	0.42	0.07	0.26
Hf	0.57	0.34	0.13	0.24	0.32	0.03	0.16
Mo	0.00	0.00	0.00	0.00	0.00	0.00	0.00
C	0.43	0.24	0.23	0.14	0.26	0.01	0.11

Post solution treatment and etching EDS analysis

Element	Point 1	Point 2	Point 3	Average wt%	Var	stdev
Ta	100.00	100.00	100.00	100.00	0.00	0.00
Hf	0.00	0.00	0.00	0.00	0.00	0.00
Mo	0.00	0.00	0.00	0.00	0.00	0.00

Note: EDS spectroscopy is not reliable for lighter weight elements when the accelerating voltage is greater than 10KeV. As a result carbon readings are inaccurate. [9]

Dilatometer Testing

Trial #	Sample #	Soultionized	Heating Rate °/min	Temp °C	Hold Time min	Cooling Rate sec
1	1	No	100	1100	2	2
2	2	No	100	1100	2	2
3	3	No	100	1100	2	2
4	4	No	100	1100	2	2
5	5	Yes	100	1100	2	2
6	1	Yes	100	1100	2	120
7	2	Yes	100	1100	10	120
8	3	Yes	100	1100	10	120
9	4	Yes	100	1100	2	960
10	5	Yes	100	1100	10	960

Table 1

Vickers Hardness Results

	test1	test2	test3	test4	Average	Var	stdev
Sintered	313	166	753	841	518.25	81370.7	285
Tungsten Furnace							
Pre-Solution	239	273	367	435	328.5	5978.75	77.3
Post-Solution	369	303	298	369	334.75	1176.19	34.3

Table 2

Processing Flow Chart 1 and 2

-Sample Preparation

37.2 weight % Ta required for phase transformation at 700°C

↓

Weighed Ta powder 13.9g: Hf powder 29g

↓

Powders mixed in N_2 atmosphere

↓

Ball Milled with steel ball bearings for 30 min.

↓

Isostaticly Pressed at 50,000 lbs

↓

4 samples:12.2g, 9.9g, 8.7g, 6.4g

-Tungsten Furnace Treatment

2 samples placed in glove bag and loaded into graphite crucible

↓

Crucible placed in furnace in Mo wire basket

↓

Furnace pumped down and backfilled with Ar

↓

Furnace heated to 2600°C in Ar

↓

Temperature held for 5 minutes

↓

Cast sample cooled by gas

↓

5 samples cut by EDM

↓

Samples solutionized for 1hr. at 1200°C in Ar gas

↓

Samples cooled by oil quenching

↓

Testing

Processing Flow Chart 3 and 4

-High Temperature Ar Furnace Treatment

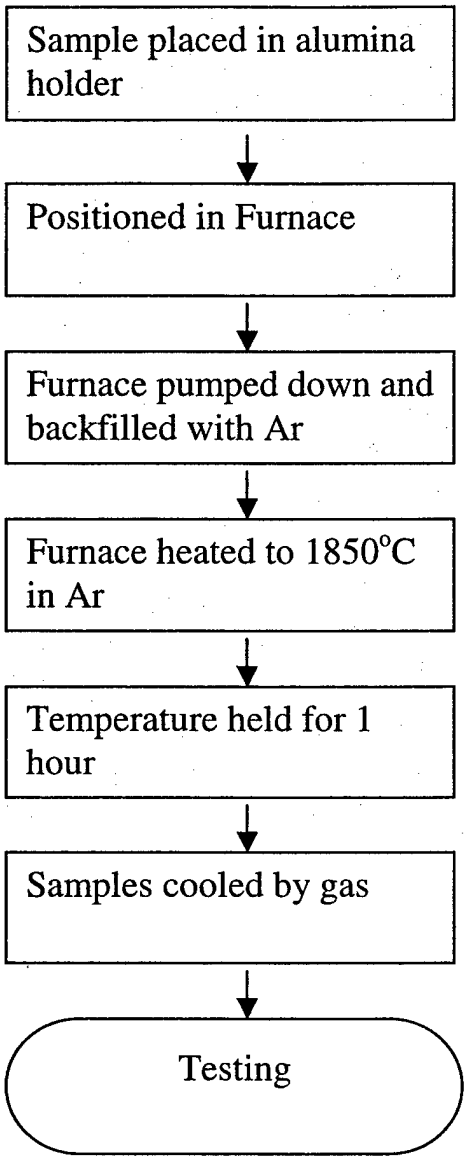

-Testing Routine